Theoretical Guarantees for the Statistical Finite Element Method*

Yanni Papandreou† Jon Cockayne ‡ Mark Girolami §
Andrew B. Duncan¶

November 16, 2021

The statistical finite element method (StatFEM) is an emerging probabilistic method that allows observations of a physical system to be synthesised with the numerical solution of a PDE intended to describe it in a coherent statistical framework, to compensate for model error. This work presents a new theoretical analysis of the statistical finite element method demonstrating that it has similar convergence properties to the finite element method on which it is based. Our results constitute a bound on the Wasserstein-2 distance between the ideal prior and posterior and the StatFEM approximation thereof, and show that this distance converges at the same mesh-dependent rate as finite element solutions converge to the true solution. Several numerical examples are presented to demonstrate our theory, including an example which test the robustness of StatFEM when extended to *nonlinear* quantities of interest.

1 Introduction

Mathematical models based on partial differential equations (PDEs) play a central role in science and engineering. Since PDEs do not generally yield closed form solutions, approximate solutions are typically obtained via numerical methods. The Finite Element Method (FEM) [30] is one such scheme which approximates the solution by solving a

* **Funding:** This work was supported by Wave 1 of The UKRI Strategic Priorities Fund under the EPSRC Grant EP/T001569/1 and EPSRC Grant EP/W006022/1, particularly the "Ecosystems of Digital Twins" theme within those grants & The Alan Turing Institute. YP was supported by a Roth Scholarship funded by the Department of Mathematics, Imperial College London.

†Imperial College London (john.papandreou18@imperial.ac.uk)
‡The Alan Turing Institute (jcockayne@turing.ac.uk)
§The Alan Turing Institute and University of Cambridge (mag92@cam.ac.uk)
¶Imperial College London and The Alan Turing Institute (a.duncan@imperial.ac.uk)

discretised problem over a finite mesh of the PDE domain. FEM-based methods have been widely studied, and as such, rigorous estimates of the error introduced through discretisation have been obtained for various families of PDEs. In particular, these results characterise the convergence of the error to zero as a function of the size of the mesh.

Mismatch between the model and the real system can occur for a variety of reasons, for example, if the geometry of the domain is not fully resolved, if underlying processes are not completely understood, or if approximations must be introduced to reduce the model to a closed system of PDEs. Stochasticity is often introduced in models to reflect the uncertainty arising from this lack of knowledge, or simply to capture intrinsically noisy processes. In the context of PDEs, stochasticity may appear in various forms, in the initial and/or boundary conditions, in the forcing terms, in the coefficients of the PDE or even in the geometry of the domain on which the PDE is defined. The resulting governing equations, known as Stochastic Partial Differential Equations (SPDEs), can be reformulated probabilistically as a probability distribution over the space of admissible solutions. The development and analysis of numerical methods for SPDEs is a very active area of research, see [35] for a review.

The increasing prevalence of instrumentation within modern engineering systems has driven the need for tools able to combine sensor data with predictions from PDE models in a manner which can mitigate any model misspecification. This technology forms an integral part of the modern notion of a digital twin, as a means of providing effective continuous monitoring of complex engineering assets.

The recently proposed statistical finite element method (StatFEM) framework [14, 15] seeks to address this need through a statistical formulation of FEM, which permits numerical approximations of a PDE to be combined with sensor observations in a principled manner through the Bayesian formalism. Due to its general applicability and ability to provide quantification of uncertainty without expensive Monte Carlo simulations, it has established itself as an effective means of assimilating data into the large-scale PDEs which arise in civil, marine and aerospace engineering. As StatFEM is built on FEM it is itself subject to numerical discretisation error which will propagate through to any predictions made by the model. Obtaining rigorous bounds on the bias introduced by discretisation error on StatFEM predictions and their associated uncertainty is a critical gap in the literature that this work will seek to address.

1.1 Related Work

This paper is focused on providing detailed error analysis for the StatFEM method first introduced in [14, 15]. For clarity of ideas, we limit our attention to linear elliptic problems. Adapting these results to time-dependent and/or non-linear PDEs is left to future research.

There has been extensive research on deriving numerical methods for solving various classes of SPDEs. For detailed reviews of such methods the reader is referred to [20, 23, 32, 29, 34, 2]. Some of these methods, for example the Stochastic Galerkin Finite Element method (SG-FEM) and its many variants, also finds their roots in the classical

finite element method, but differ fundamentally from StatFEM. More specifically, SG-FEM methods reformulate the SPDE as a deterministic PDE on a higher dimensional domain, where additional variables are introduced to characterise the underlying noise process. On the other hand, in the StatFEM approach, the approximation is itself intrinsically stochastic. While SG-FEM methods are applicable to a wider class of SPDEs, their scalability is limited by the curse of dimensionality resulting from the augmented noise dimensions. Additionally, while StatFEM formulation permits fast assimilation of measurement data, this is not straightforward for SG-FEM and related methods.

In the area of spatial statistics, Gaussian random fields are constructed as the solution of appropriately chosen SPDEs [19]. The solution is approximated through a finite element discretisation of the weak form of the underlying SPDE. The resulting discretised solution is subsequently employed as a prior within a Bayesian inference problem for a spatial or spatio-temporal model [28]. For non-Gaussian likelihoods, fast approximate Bayesian Inference for the resulting latent Gaussian model is possible using an Integrated Nested Laplace Approximation (INLA) [21]. The construction of the StatFEM model is strongly connected to this statistical viewpoint of SPDEs. Indeed, in both cases, the spatial priors are Gaussian Markov Random Fields (GMRFs). In the case of StatFEM the mean and covariance of the GMRF reflect the behaviour of the underlying deterministic PDE, while in the SPDE case the the covariance is tailored to ensure a specific degree of spatial decorrelation of the underlying latent Gaussian random field.

Conceptually, StatFEM also bears some similarity to Probabilistic Numerics Methods [17], both being statistical reformulations of numerical methods. Indeed, PN methods have also been developed for approximating solutions of ordinary differential equations (ODEs) [33] as well as PDEs [7, 4, 5]. The two methodologies share common foundations, particularly Bayesian Probabilistic Numerical (BPN) Methods [6] which are formulated as conditioning a prior distribution of potential solutions on partial evaluations of the underlying equations. StatFEM also builds on the Bayesian formalism, employing conditioning to incorporate new information, specifically noisy sensor observations, starting from a prior which characterises the distribution of approximate PDE solutions. However, these methods fundamentally differ in what they seek to achieve: Probabilistic Numerical Methods (PNMs) methods seek to recast numerical discretisation error as uncertainty, whereas the uncertainty arising in StatFEM primarily seeks to account for model error.

1.2 Contributions

The novel contributions of the paper are as follows:

- We study the bias introduced by discretisation error in the StatFEM model, and derive rigorous upper bounds for the bias introduced in the prior and posterior in terms of the properties of the underlying finite element mesh.
- We conduct a thorough simulation study confirming our theoretical results on a number of illustrative FEM test problems.

- We empirically explore the limits of our theory by studying the bias induced by StatFEM in a scenario where the assumptions underpinning our theoretical results are no longer valid.

1.3 Structure of the Paper

The remainder of the paper is structured as follows. In Section 1.4 we introduce notation required for the rest of the paper. In Section 2 we reintroduce StatFEM, deriving it from first principles. Section 3 contains our main theoretical contributions, error bounds for the StatFEM prior and the posterior when this prior is conditioned on sensor observations. We conduct simulations verifying our theoretical results in Section 4, and providing some concluding remarks in Section 5. The supplementary material contains the proofs required for the paper in Section S2.

1.4 Notation

In this section we introduce required notation for the remainder of the paper. Given a normed space $\mathcal{X}$ denote the associated norm by $\|\cdot\|_{\mathcal{X}}$. Given two normed spaces $\mathcal{X}, \mathcal{Y}$ we denote by $L(\mathcal{X}, \mathcal{Y})$ the set of all bounded linear operators from $\mathcal{X}$ to $\mathcal{Y}$. We denote the dual of $\mathcal{X}$ by $\mathcal{X}' = L(\mathcal{X}, \mathbb{R})$. When $\mathcal{X}$ is a Hilbert space we denote the associated inner product by $\langle \cdot, \cdot \rangle_{\mathcal{X}}$. We will sometimes drop the subscript for the norm and inner product when there is no risk of confusion over which spaces we are referring to.

Let $\mathcal{X}, \mathcal{Y}$ be Hilbert spaces. Given an operator $A \in L(\mathcal{X}, \mathcal{Y})$ we denote the adjoint of A by $A^\dagger \in L(\mathcal{Y}, \mathcal{X})$. Given $A \in L(\mathcal{X}, \mathcal{X})$, we say that A is symmetric if $A = A^\dagger$ and positive definite if it is symmetric and $\langle x, Ax \rangle > 0$ for all nonzero $x \in \mathcal{X}$. Recall that the trace of A can be defined as $\mathrm{tr}(A) = \sum_{i=1}^{\infty} \langle Ae_i, e_i \rangle$ where $\{e_i\}_{i=1}^{\infty}$ is any orthonormal basis of $\mathcal{X}$. We will say that $A \in L(\mathcal{X}, \mathcal{X})$ is trace-class if $\mathrm{tr}(A) < \infty$. For an operator $A : \mathcal{X} \to \mathcal{Y}$ we will define the operator norm to be $\|A\|_{\mathcal{X} \to \mathcal{Y}} = \sup_{x \in \mathcal{X}} \frac{\|Ax\|_{\mathcal{Y}}}{\|x\|_{\mathcal{X}}}$, the trace norm to be $\|A\|_{\mathrm{tr}} = \mathrm{tr}([A^\dagger A]^{1/2})$, while the Hilbert-Schmidt norm is defined to be $\|A\|_{\mathrm{HS}} = \mathrm{tr}(A^\dagger A)^{1/2}$. Recall the well known inequality $\|A\|_{\mathcal{X} \to \mathcal{Y}} \leq \|A\|_{\mathrm{HS}} \leq \|A\|_{\mathrm{tr}}$.

Let $D \subset \mathbb{R}^d$ be an open domain with boundary ∂D and let $\overline{D} = D \cup \partial D$ be its closure. We denote by $C(D), C(\overline{D})$ the space of continuous functions on D and $\overline{D}$, respectively. Denote by $L^p(D)$ the spaces of p-integrable functions on D and $W^{k,p}(D)$ the Sobolev space with p-integrable derivatives up to and including order k. We use the notation $H^k(D) = W^{k,2}(D)$ and $H_0^k(D)$ to be the elements of $H^k(D)$ which are zero on ∂D. For clarity we will often use the notation $\|\cdot\|_k$, $|\cdot|_k$ to denote the norm and semi-norm associated to $H^k(D)$.

1.5 Relevant Probability-Theoretic Concepts

In this section we briefly introduce and discuss the relevant probability-theoretic concepts we will require. To this end, for a space $\mathcal{X}$ let $\mathcal{B}(\mathcal{X})$ denote the Borel sigma-algebra of $\mathcal{X}$, and for a measurable space $(\mathcal{X}, \mathcal{B}(\mathcal{X}))$ let $\mathcal{P}(\mathcal{X})$ denote the set of all Borel probability measures on $\mathcal{X}$.

Given a positive definite kernel function $k : D \times D \to \mathbb{R}$ on the domain D, and a function $m : D \to \mathbb{R}$ we say f is a Gaussian process with mean function m and covariance function k if for every finite collection of points $\{x_1, \ldots, x_N\} \subset D$ the random vector $(f(x_1), ..., f(x_N))$ is a multivariate Gaussian random variable with mean vector $(m(x_1), ..., m(x_N))$ and covariance matrix $\{k(x_n, x_m)\}_{n,m=1,...,N}$. The mean function and kernel/covariance function completely determine the Gaussian process. We write $f \sim \mathcal{GP}(m, k)$ to denote the Gaussian process with mean function m and covariance function k. We refer the reader to [26] for further details.

Gaussian processes that take values in a separable Hilbert space $\mathcal{X}$ can be associated canonically with a Gaussian measure on the space $\mathcal{X}$. Gaussian measures on infinite-dimensional Hilbert spaces can be viewed as a generalisation of their finite-dimensional counterpart on $\mathbb{R}^d$, and are defined by a mean element $m \in \mathcal{X}$ and covariance operator K, which is a positive-definite trace class operator. See [10] and [3] for more information. Given a Gaussian process $f \sim \mathcal{GP}(m, k)$, this can be associated with the Gaussian measure $\mathcal{N}(m, K)$ with mean m and covariance operator K, associated with the kernel k, defined by

$$Kg(\cdot) = \int k(\cdot, y)g(y)\, dy, \quad g \in \mathcal{X}.$$

Given any $m \in \mathcal{X}$ and $K \in \mathcal{L}(\mathcal{X}, \mathcal{X})$ which is positive-definite and trace class, there exists a Gaussian measure $\mathcal{N}(m, K)$ with mean m and covariance operator K [10, Proposition 2.18].

For the purposes of studying the error in StatFEM we will need to introduce a metric on the space of distributions. The probability metric we will work with in this paper is the Wasserstein distance; this will be justified in Section 3. Given two probability measures μ, ν on a normed space $\mathcal{X}$, having the first two moments finite, the Wasserstein-2 distance between the two measures, $W_2(\mu, \nu)$, is defined as:

$$W_2^2(\mu, \nu) = \inf_{\pi \in \Gamma(\mu,\nu)} \int_{\mathcal{X}\times\mathcal{X}} \|x - y\|_{\mathcal{X}}^2 \mathrm{d}\pi(x, y) \tag{1}$$

where $\Gamma(\mu, \nu)$ is the set of couplings of μ and ν, i.e.

$$\Gamma(\mu, \nu) = \{\pi \in \mathcal{P}(\mathcal{X} \times \mathcal{X}) \mid \pi(E \times \mathcal{X}) = \mu(E) \text{ and } \pi(\mathcal{X} \times F) = \nu(F) \text{ for all } E, F \in \mathcal{B}(\mathcal{X})\}.$$

Throughout we will abbreviate $W_2(\mu, \nu) = W(\mu, \nu)$.

It will be also useful to note that the Wasserstein distance between the measures μ, ν above can be linked to the Wasserstein distance between the centered measures. Let m denote the expectation of μ; then the centered measure μ^* is defined by

$$\mu^*(E) = \mu(\{x - m \mid x \in E\})$$

for all $E \in \mathcal{B}(\mathcal{X})$. Denoting the means of μ, ν by m_1, m_2 respectively we have from [9]:

$$W^2(\mu, \nu) = \|m_1 - m_2\|_{\mathcal{X}}^2 + W^2(\mu^*, \nu^*). \tag{2}$$

We also recall that there is an explicit expression for the Wasserstein distance between two Gaussians. Let $\mu_i = \mathcal{N}(m_i, \Sigma_i), i = 1, 2$ be two Gaussian measures on a separable Hilbert space $\mathcal{X}$. Then from [22], we have

$$W^2(\mu_1, \mu_2) = \|m_1 - m_2\|_{\mathcal{X}}^2 + \mathrm{tr}(\Sigma_1) + \mathrm{tr}(\Sigma_2) - 2\,\mathrm{tr}\sqrt{\Sigma_1^{1/2}\Sigma_2\Sigma_1^{1/2}}. \tag{3}$$

2 The Statistical Finite Element Method

In this section we will present the StatFEM model. We begin by reviewing FEM in Section 2.1. Then, in Section 2.2 we will derive the prior distribution over the solution to the PDE that is used in StatFEM. Finally, in Section 2.3 we will condition this prior distribution on sensor observations to obtain the StatFEM posterior distribution.

2.1 The Finite Element Method

In this section we will briefly review the necessary concepts from FEM needed for StatFEM, focusing on elliptic PDEs. We begin by establishing notation. Consider the following linear elliptic boundary value problem (BVP):

$$\begin{aligned} \mathcal{L}f(x) := -\nabla \cdot (\kappa(x)\nabla u(x)) &= f(x) \qquad x \in D \\ u(x) &= 0 \qquad x \in \partial D, \end{aligned} \tag{4}$$

for some positive, spatially-dependent conductivity $\kappa : D \to \mathbb{R}_{>0}$ and forcing $f \in L^2(D)$. We make the following assumptions on the the *data* (D, κ, f):

Assumption 1 (domain regularity)**.** The dimension of the domain is restricted to $d \in \{1, 2\}$. The domain D is convex polygonal, i.e. it is convex and its boundary ∂D is a polygon. Note that this implies that the domain is bounded. ♦

Assumption 1 is assumed for simplicity; we note that it should be possible to relax some of these assumptions though this is not investigated in this work.

Assumption 2 (parameter regularity)**.** The parameter κ is a continuous function on $\overline{D}$, i.e. $\kappa \in C(\overline{D})$. Further, there exists a constant $\alpha > 0$ such that:

$$\kappa(x) \geq \alpha > 0, \quad \text{for almost all } x \in D \tag{5}$$

Inequality Eq. (5) is often referred to as *(uniform) ellipticity* of the parameter. ♦

We consider the *weak solution* of the BVP Eq. (4), namely we seek $u \in H_0^1(D)$ which satisfies the variational formulation of Eq. (4), i.e.

$$\int_D \nabla v(x) \cdot (\kappa(x)\nabla u(x))\,\mathrm{d}x = \int_D f(x)v(x)\mathrm{d}x, \quad \forall v \in H_0^1(D) \tag{6}$$

Under Assumptions 1 and 2, standard regularity results [12, section 6.2.2] show that, for each $f \in L^2(D)$, there exists a unique *weak solution* $u \in H_0^1(D)$ satisfying Eq. (6).

Further, Assumptions 1 and 2 guarantee stronger regularity of the weak solution. From [18, section 3.7] it holds that $u \in H^2(D)$ and that there exists a constant $\tilde{C} > 0$ such that $\|u\|_2 \leq \tilde{C}\|f\|_{L^2(D)}$. Note that this extra regularity can be generalised to elliptic problems in higher dimensions [16, Theorem 3.2.1.2]

We can reformulate the variational formulation Eq. (6) as

$$a(u, v) = \langle f, v \rangle \quad \forall v \in H_0^1(D) \tag{7}$$

where the bilinear form $a : H_0^1(D) \times H_0^1(D) \to \mathbb{R}$ is defined by

$$a(u, v) := \int_D \nabla v(x) \cdot (\kappa(x) \nabla u(x)) \, \mathrm{d}x \tag{8}$$

Assumption 2 on κ ensures that the bilinear form a is symmetric, bounded and coercive [12].

The *Galerkin approximation* of the variational problem (7) seeks an approximate solution $u_h \in V_h$ within a finite dimensional subspace V_h of $H_0^1(D)$ which satisfies

$$a(u_h, v) = \langle f, v \rangle, \quad \forall v \in V_h.$$

The construction of the finite element method arises from a specific Galerkin approximation, where we introduce a *triangulation* of the domain, $\mathcal{T}_h = \{\omega_e\}_{e=1}^{n_e}$, where the ω_e are pairwise disjoint triangular elements with $D = \cup_{e=1}^{n_e} \omega_e$, and h is the diameter of the largest element. This triangulation is usually referred to as the finite element mesh (FE mesh) and we will refer to h as the *mesh width*. The discrete function space V_h is then chosen to be piecewise polynomial functions defined on this mesh. The approximate weak solution u_h can be expressed as a linear combination of basis functions $\{\phi_i\}_{i=1}^{n_u}$. In this work, we assume that V_h is the space of piecewise continuous functions, and $\{\phi_i\}_{i=1}^{n_u}$ chosen to be a *nodal basis* which satisfies $\phi_i(x_j) = \delta_{ij}$, where $x_1, \ldots, x_{n_u}$ are the internal vertices of the mesh.

By exploiting the linearity of both the bilinear form and the inner product in Eq. (7) the FEM discretisation of the variational formulation of our BVP yields the following discrete system of linear equations:

$$A\mathbf{u} = \mathbf{f} \tag{9}$$

where $A \in \mathbb{R}^{n_u \times n_u}$ is the *stiffness matrix* whose ij*-th* element is given by:

$$A_{ij} = a(\phi_j, \phi_i) = \int_D \nabla \phi_i \cdot (\kappa(x) \nabla \phi_j) \mathrm{d}x \tag{10}$$

The vector $\mathbf{u} \in \mathbb{R}^{n_u}$ is the vector of degrees of freedom (DOFs) and $\mathbf{f} \in \mathbb{R}^{n_u}$ is the *load vector* whose i*-th* entry is given by:

$$f_i = \langle f, \phi_i \rangle = \int_D f \phi_i \mathrm{d}x \tag{11}$$

The *stiffness matrix*, A, is a real symmetric matrix which is invertible by Assumption 2 [20, see Theorem 2.16]. Thus, the system of linear equations Eq. (9) can be solved for $\mathbf{u}$,

yielding the finite element approximation $u_h = \mathbf{\Phi}^T \mathbf{u}$ where $\mathbf{\Phi} := (\phi_1, \cdots, \phi_{n_u})^T$ is the vector of the FE basis functions. The *mass matrix*, $M \in \mathbb{R}^{n_u \times n_u}$ which is defined by

$$M_{ij} = \langle \phi_i, \phi_j \rangle = \int_D \phi_i \phi_j \mathrm{d}x, \tag{12}$$

will also play an important role in the error analysis of Section 3.

It will be important for our work to have access to a bound on the error between the true solution and the FEM approximation in terms of h. To this end consider a family of triangulations $\{\mathcal{T}_{h_i}\}$, such that $h_i \to 0$ and $h_i > 0$ for all i. We will require a further technical assumption on the family of the FE meshes:

Assumption 3. The meshes under consideration remain regular in the sense that as we decrease h_i to 0 the angles of all triangles are bounded below independently of h_i. ♦

Under the assumptions above we have the following classical H^1 error bound [18, see chapter 5]:

Theorem 1. *Let u be the unique weak solution to BVP Eq. (4) and let u_h by the FEM approximation. Assume that $f \in L^2(D)$ and that the Assumptions 1 to 3 hold. We then have the following H^1 error bound, for sufficiently small h:*

$$|u - u_h|_1 \leq Ch\|u\|_2 \tag{13}$$

where $C > 0$ is a positive constant independent of h. ♦

From this H^1 error bound a standard duality argument yields the following L^2 error bound [18, see chapter 5], which will play an important role in the error analysis of Section 3.

Theorem 2. *Let u be the unique weak solution to BVP Eq. (4) and let u_h by the FEM approximation. Assume that $f \in L^2(D)$ and that the Assumptions 1 to 3 hold. We then have the following error bound, for sufficiently small h:*

$$\|u - u_h\|_{L^2(D)} \leq Ch^2\|f\|_{L^2(D)} \tag{14}$$

where $C > 0$ is a positive constant independent of h. ♦

2.2 The StatFEM Prior

In this section we present the StatFEM approximation for the solution of a stochastically-forced elliptic PDE. The resulting probability distribution will subsequently be employed as a prior to be combined with sensor data through Bayesian updates. To this end, we consider the BVP Eq. (4) where f is chosen to be a Gaussian process (GP),

$$f \sim \mathcal{GP}(\bar{f}, k_f),$$

where $\bar{f} \in C(D)$ and where we assume the covariance k_f is regular enough so that realisations of f lie almost surely in $L^2(D)$. It is sufficient to take $k_f(x, y) = \psi(x - y)$

where $\psi : D \to \mathbb{R}$ is continuous [27, see Corollary 1]. This is satisfied for example by the RBF kernel or any kernel in the Matérn family. Another alternative sufficient condition would be to choose the kernel so that the associated covariance operator is an appropriate negative power of the Laplacian. This is outlined in detail in [31, see section 6].

In our analysis we shall assume that the conductivity coefficient κ is deterministic, unlike [15] where this is assumed to be stochastic. Since Eq. (4) is well-posed, the solution can be expressed as $u = \mathcal{L}^{-1}f$, where $\mathcal{L}^{-1}$ is the inverse of the differential operator $\mathcal{L}$. The pushforward of the probability measure for f through $\mathcal{L}^{-1}$ induces a probability distribution of solutions supported on $H_0^1(D)$. Since the inverse operator is linear, the resulting distribution for u will also be a Gaussian measure supported on $L^2(D)$, with mean $\mathcal{L}^{-1}\overline{f}$ and covariance operator $\mathcal{L}^{-1}K\mathcal{L}^{-1}$, where K is the covariance operator of f on $L^2(D)$. Indeed, u can be expressed as a Gaussian process [25, Proposition 3.1]

$$u \sim \mathcal{GP}(\mathcal{L}^{-1}\bar{f}, k_{\mathcal{L}}) \tag{15}$$

where

$$k_{\mathcal{L}}(x, y) = \mathcal{L}_x^{-1}\mathcal{L}_y^{-1}k_f(x, y).$$

Here $\mathcal{L}_x^{-1}$ denotes the action of the operator $\mathcal{L}^{-1}$ on the first argument of the kernel and $\mathcal{L}_y^{-1}$ its action on the second argument.

We intend to use Eq. (15) as a prior, which will later be combined with sensor observations through sequential Bayesian updates. An important observation is that the mean and covariance of the GP defined in Eq. (15) cannot be computed exactly for general problems, which precludes the calculation of marginal distributions or realisations of the GP. To overcome this issue, another GP, which employs a finite element approximation of the mean and covariance functions will be introduced.

As discussed in Section 2.1 FEM approximates the solution to our elliptic BVP as a linear combination of the FE basis functions. In particular, the FEM approximation to the solution of our elliptic BVP can be expressed as follows:

$$u_h = \mathbf{\Phi}^T A^{-1}\mathbf{f} =: \hat{L}_h^{-1} f \tag{16}$$

where the operator $\hat{L}_h^{-1} : L^2(D) \to L^2(D)$ is defined as $\hat{L}_h^{-1} := \mathbf{\Phi}^T A^{-1}\mathcal{F}_h$. Here the operator $\mathcal{F}_h : L^2(D) \to \mathbb{R}^{n_u}$ takes a function f to the load vector $\mathbf{f}$, defined in Eq. (11), and A is the stiffness matrix defined in Eq. (10). The StatFEM approximation to (15) is obtained by formally replacing the solution operator $\mathcal{L}^{-1}$ with $\hat{L}_h^{-1}$ in the mean and covariance terms. Due to the linearity of the approximation solution map, the resulting process is still a Gaussian process, with transformed mean and covariance.

Proposition 1. *The StatFEM prior from [14, 15] is a GP of the form*

$$u_h \sim \mathcal{GP}(\bar{u}_h, k_h) \tag{17}$$

where the mean and covariance function are defined by:

$$\bar{u}_h(x) := \mathbf{\Phi}(x)^T A^{-1}\bar{\mathbf{f}} \tag{18}$$

$$k_h(x, y) := \mathbf{\Phi}(x)^T A^{-1} K_{\mathcal{F}_h} A^{-1}\mathbf{\Phi}(y) \tag{19}$$

where $K_{\mathcal{F}_h} := \mathcal{F}_h K \mathcal{F}_h^\dagger \in \mathbb{R}^{n_u \times n_u}$ *and* $\bar{\mathbf{f}} := \mathcal{F}_h \bar{f} \in \mathbb{R}^{n_u}$. ♦

The question of how much error is introduced by replacing u with u_h can be formulating as quantifying the distance between the probability measures associated with each Gaussian process. To this end, we define ν_* and ν_h to be the Gaussian probability measures supported on $L^2(D)$ which are associated with the GPs (15) and (17), respectively. We can write $\nu_* = \mathcal{N}(m_*, \Sigma_*)$ and $\nu_h = \mathcal{N}(m_h, \Sigma_h)$ where

$$\begin{aligned} m_\star &= \mathcal{L}^{-1} \bar{f} \\ \Sigma_\star &= \mathcal{L}^{-1} K \mathcal{L}^{-\dagger}, \end{aligned}$$

and

$$\begin{aligned} m_h &= \hat{L}_h^{-1} \bar{f} \\ \Sigma_h &= \hat{L}_h^{-1} K \hat{L}_h^{-\dagger}. \end{aligned}$$

Remark 1. Let $V_\star, V_h$ be the supports of $\nu_\star, \nu_h$ respectively. Since the image of the approximate solution operator $\hat{L}_h^{-1}$ is the span of the FE basis functions $\{\phi_i\}_{i=1}^{n_u}$ it follows that, for all $h > 0$, V_h is a finite dimensional subspace of $H_0^1(D) \subseteq L^2(D)$. Further, under Assumptions 1 and 2 we have that $V_\star$ is an infinite dimensional subspace of $H_0^1(D) \subseteq L^2(D)$. In the case that V_h and $V_\star$ are disjoint we clearly have that $\nu_\star$ and ν_h are mutually singular. Consider now the case that V_h and $V_\star$ are not disjoint and $V_h \not\subseteq V_\star$. This means that V_h and $V_\star$ have a non-empty intersection, and that there exists a subset $\widetilde{V} \subseteq V_\star$ not in the intersection. Further, ν_h gives 0 measure to $\widetilde{V}$, while $\widetilde{V}$ has positive measure under $\nu_\star$. This implies that $\nu_\star$ and ν_h are mutually singular. Finally, in the case that $V_h \subset V_\star$ we can write $V_\star$ as the orthogonal direct sum of V_h and its complement. Since ν_h gives full measure to V_h it must give measure 0 to the orthogonal complement of V_h, which has positive measure under $\nu_\star$. Hence, we again have that $\nu_\star$ and ν_h are mutually singular. In all cases, the mutual singularity follows from the Feldman-Hajek theorem [10, Theorem 2.25].

2.3 Posterior Updates of the StatFEM approximation

We now consider the problem of inferring the solution u of the BVP (4) for an unknown forcing term f based on noisy observations of the form

$$\mathbf{v} = Su + \boldsymbol{\xi}, \quad \boldsymbol{\xi} \sim \mathcal{N}(0, \epsilon^2 I) \tag{20}$$

where S is a linear observation map. Following the Bayesian formalism [31], the solution of this inverse problem is characterised by the posterior distribution $\widetilde{\nu}_*(du)$ of u given the observations $\mathbf{v}$,

$$\widetilde{\nu}_*(du) \propto e^{-\Phi(\mathbf{v};u)} \nu_*(du) \tag{21}$$

where $\Phi(\mathbf{v}; u) = \frac{1}{2\epsilon^2} \|Su - \mathbf{v}\|^2$, is the negative log-likelihood, and ϵ is the observational noise standard deviation. In practice, we would work with an alternative posterior distribution, where the prior distribution $\nu_\star$ is replaced with a prior obtained from a finite

element approximation. To understand the consequences of making this approximation, we must quantify the distance (in an appropriate sense) between the posterior probability measures (21) and

$$\widetilde{\nu}_h(du) \propto e^{-\Phi(\mathbf{v};u)}\nu_h(du). \tag{22}$$

We shall make the following assumptions, on the observation map S.

Assumption 4. The observation map $S : C(D) \to \mathbb{R}^s$ is a bounded linear operator with full range.

Remark 2. Note that the assumptions on the covariance structure of the forcing f guarantee that solutions to our noisy elliptic BVP lie in $H^2(D)$ almost surely. Thus, the support of the true prior lies in $H^2(D)$. By the Sobolev Embedding Theorem for dimensions 1,2, one has that $H^2(D) \subset C(D)$ so that S is well-defined for functions drawn from the true prior. Draws from the StatFEM prior are trivially in $C(D)$ and so S is well-defined for functions drawn from this prior as well. Note that the condition on the range of S will always be true for some $s > 0$.

A property which will be very important for the subsequent error analysis of Section 3 is that the posterior distributions $\widetilde{\nu}_*$ and $\widetilde{\nu}_h$ remain Gaussian measures. This can be viewed as the infinite dimensional version of the analogous result for multivariate Gaussians based on "completing the square".

Proposition 2. *Suppose that the observation map satisfies Assumption 2 and let* $\mathbf{v} \in \mathbb{R}^s$. *Then* $\widetilde{\nu}_*$ *and* $\widetilde{\nu}_h$ *are Gaussian measures with mean and covariance given by*

$$m_{u|\mathbf{v}}^{(a)} := m_a + \Sigma_a S^\dagger(\epsilon^2 I + S\Sigma_a S^\dagger)^{-1}(\mathbf{v} - Sm_a) \tag{23}$$

$$\Sigma_{u|\mathbf{v}}^{(a)} := \Sigma_a - \Sigma_a S^\dagger(\epsilon^2 I + S\Sigma_a S^\dagger)^{-1} S\Sigma_a, \tag{24}$$

respectively, for $a \in \{*, h\}$. ♦

3 Discretisation Error Analysis

Intuitively we expect that $\nu_h \to \nu_\star$ as $h \to 0$ in an appropriate sense because of the convergence properties of the finite element discretisation. Similarly, we expect that the approximate posterior, $\tilde{\nu}_h$, will converge to the true posterior, $\tilde{\nu}_\star$, in an appropriate sense, as $h \to 0$.

To establish these properties we must select an appropriate metric for the distance between the priors and posteriors. A challenge with selecting this metric is that, as explained in Remark 1, the measures $\{\nu_h, \nu_\star\}$ and $\{\tilde{\nu}_h, \tilde{\nu}_\star\}$ are generally mutually singular. This complicates the typical stability analysis that arises when studying Bayesian inverse problems, based on Kullback-Leibler divergence or Hellinger distance [8]. In this paper we shall adopt an alternative approach, employing the Wasserstein-2 metric to quantify the influence of discretisation error on the posterior distribution. This is advantageous in this context for several reasons: firstly it is not dependent on the use of a common

dominating measure. Secondly, unlike other divergences, it is robust under vanishing noise: in this limit, the Wasserstein distance between the two probability measures will converge to the deterministic L^2 discretisation error between the respective two means. Finally, while computing Wasserstein distance is intractable for general measures, there exists a closed form for the Wasserstein-2 distance between Gaussian measures, valid in both finite and infinite dimensions. See [22] for a statement of this and see [11, 24] for proofs in the finite dimensional case, and [9] for a proof in the infinite dimensional case.

The results in this section will focus on bounding the Wasserstein distance between the priors ν_* and ν_h, and the posteriors $\widetilde{\nu}_*$ and $\widetilde{\nu}_h$ as a function of h. The strategy employed to obtain these bounds involves exploiting an important connection between Wasserstein distance between Gaussian measures on Hilbert spaces and the Procrustes Metric between the respective covariance operators, as detailed in [22]. We now present these results in the following two theorems.

Theorem 3 (Prior Error Analysis)**.** *Assuming that $f \in L^2(D)$, and that the domain, D, and parameter, κ, satisfy Assumptions 1 to 3 there exists a constant $\gamma > 0$, independent of h, such that, for sufficiently small h we have:*

$$W(\nu_\star, \nu_h) \leq \gamma h^2 \tag{25}$$

♦

The next theorem describes how this error in the prior propagates forward to the error between arbitrary linear functionals of the true and StatFEM posterior, again as a function of the mesh width h.

Theorem 4 (Posterior Error Analysis)**.** *Let $\ell : L^2(D) \to \mathbb{R}$ be a bounded linear functional. Assuming that $f \in L^2(D)$, and that the domain, D, and parameter, κ, and the observation map S, satisfy Assumptions 1 to 4 there exists a constant $\gamma'(\ell) > 0$, independent of h, such that, for sufficiently small h we have:*

$$W(\ell\tilde{\nu}_\star, \ell\tilde{\nu}_h) \leq \gamma'(\ell)h^2 + \mathcal{O}(h^4) \text{ as } h \to 0 \tag{26}$$

♦

Remark 3. Theorem 4 provides a bound on $W(\ell\tilde{\nu}_\star, \ell\tilde{\nu}_h)$, for arbitrary ℓ, rather than on $W(\tilde{\nu}_\star, \tilde{\nu}_h)$. Naturally a bound on the latter quantity is stronger and more of interest, but deriving such a bound is technically challenging. Nevertheless the empirical results in Section 4 suggest that the stronger result may hold, and as a result this will be the focus of future research. ♦

Theorem 3 shows that we have control over the Wasserstein distance between the full priors while Theorem 4 shows that, in the posterior case, we have control over linear quantities of interest. Nonlinear quantities of interest are also interesting and we will explore whether they are controlled empirically in the numerical experiments in Section 4.

4 Experiments

In this section we will present some numerical experiments demonstrating the theoretical results from Section 3. In Section 4.1 we will consider a one-dimensional example in which we have access to an explicit formula for the Green's function, while in Section 4.2 we will consider a more challenging two-dimensional problem in which the solution operator is not available. In both scenarios we will aim to demonstrate the StatFEM prior and posterior bounds. Note that while Theorem 4 shows only that $W(\ell\tilde{\nu}_\star, \ell\tilde{\nu}_h)$ is $\mathcal{O}(h^2)$ our experiments suggest that for the problems examined here it also holds that $W(\tilde{\nu}_\star, \tilde{\nu}_h)$ is $\mathcal{O}(h^2)$. Finally, in Section 4.3 we explore whether our convergence results extend beyond the linear setting by calculating the Wasserstein distance between the prior and posterior distributions of a *nonlinear* quantity of interest, given by $\max_{x\in D} u(x)$. The code for these numerical experiments is available online[1]. Additional implementation details for the experiments are provided in Section S1.

4.1 One-dimensional Poisson Equation

In this section we will present a numerical experiment involving the following one-dimensional Poisson equation:

$$\begin{aligned} -\frac{d^2u}{dx^2}(x) &= f(x) \quad x \in [0,1] \\ u(0) &= u(1) = 0 \end{aligned} \tag{27}$$

where the forcing f is distributed as,

$$f \sim \mathcal{GP}(\bar{f}, k_f) \tag{28}$$

with mean and covariance function given by:

$$\bar{f}(x) = 1 \tag{29}$$

$$k_f(x,y) = \sigma_f^2 \exp\left(-\frac{|x-y|^2}{2l_f^2}\right). \tag{30}$$

We took $\sigma_f = 0.1$ and $l_f = 0.4$. Note that the BVP Eq. (27) is an instance of the general problem Eq. (4) with $d = 1$, $D = [0,1]$, and $\kappa(x) \equiv 1$. The Green's function, $G(x,y)$, for the BVP Eq. (27) is easily computed to be:

$$G(x,y) = x(1-y)\Theta(y-x) + (1-x)y\Theta(x-y) \quad \forall x, y \in [0,1] \tag{31}$$

where $\Theta(x)$ is the Heaviside Step function. As discussed in Section 2.2 the solution u to problem Eq. (27) will be the Gaussian process defined by Eq. (15). Since we readily have the Green's function available for our 1D problem we can explicitly write down this distribution as:

$$u \sim \mathcal{N}(\mu_\star, k_\star) \tag{32}$$

[1] https://github.com/YanniPapandreou/statFEM

where the mean and covariance functions are given by:

$$\mu_\star(x) = \int_0^1 G(x,w)\bar{f}(w)\mathrm{d}w = \frac{1}{2}x(1-x), \tag{33}$$

$$k_\star(x,y) = \int_0^1 \int_0^1 G(x,w)k_f(w,t)G(t,y)\mathrm{d}t\mathrm{d}w \tag{34}$$

Note that we have explicitly computed the integral for the mean $\mu_\star$, but not for the covariance $k_\star$. The double integral for the covariance is approximated numerically using quadrature to accurately compute this on a reference grid.

4.1.1 Prior results for 1-D example

Since we can straightforwardly evaluate the true prior numerically, we can now demonstrate the error bound for the StatFEM prior given in Theorem 3. In order to do this the following remark, taken from [1], will be useful.

Remark 4. When we have access to the true distributions we can estimate the rate of convergence of the StatFEM priors and posteriors as follows. Let $\eta_\star, \eta_h$ denote the true and StatFEM prior (or posterior) respectively. If we assume that we have a rate of convergence p, i.e.,

$$W(\eta_\star, \eta_h) \leq \mathcal{O}(h^p) \text{ as } h \to 0 \tag{35}$$

then we have that there is a constant $C > 0$, independent of h, such that,

$$W(\eta_\star, \eta_h) = Ch^p + \mathcal{O}(h^{p+1}) \tag{36}$$

from which it follows that,

$$\log W(\eta_\star, \eta_h) = p \log h + \log |C| + \mathcal{O}(h) \tag{37}$$

From this we can see that we can estimate the rate of convergence, p, when we know the true distributions by computing the Wasserstein distance for a range of sufficiently small h-values, plotting a log-log plot of these values, and estimating the slope of the line of best fit. ♦

As outlined in Remark 4 above we compute, for a range of sufficiently small h-values, an approximation of the Wasserstein distance between the two priors and then plot these results on a log-log scale. We take a reference grid of $N = 51$ equally spaced points in $[0, 1]$ to compare the covariances, and we take 30 h-values in $[0.02, 0.25]$. With these choices we obtain the plot shown in Fig. 1 below. From this plot we can see that the results indeed lie along a straight line with a slope estimated to be $p = 2.00$ (to 2 decimal places) using `scipy`'s built in linear regression function.

4.1.2 Posterior results for 1-D example

For this example we will consider a specific case of the general Bayesian inverse problem outlined in Section 2.3 which will correspond to taking the observation operator S to

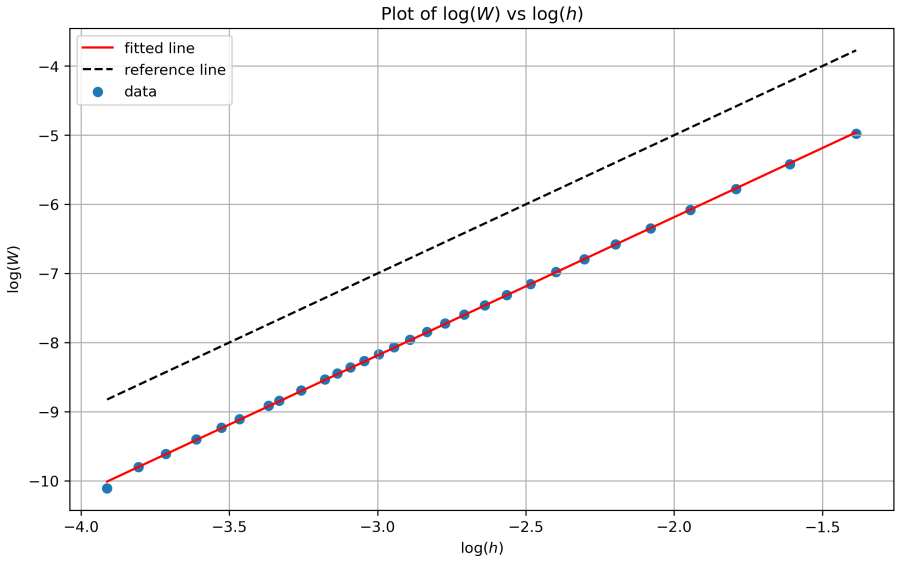

Figure 1: Log-log plot of Wasserstein distance against h for the priors in a 1-D example. The reference line has a slope of 2. The slope of the fitted line is estimated to be $p = 2.00$, in agreement visually with the reference line.

be a pointwise evaluation operator. More specifically, we suppose that we have sensor data which correspond to noisy observations of the value of the solution u at some points $\{y_i\}_{i=1}^s \subset D$. We thus take S to be the operator which maps a function g to the vector $Sg := (g(y_1), \ldots, g(y_s))^T \in \mathbb{R}^s$. For this choice of S the update equations for the posterior means and covariances given in Eqs. (23) and (24) respectively can be simplified to a form which is more amenable to computation. These forms, for i being either the symbol $\star$ or h, are:

$$m^{(i)}_{u|\mathbf{v}}(x) = m_i(x) - \mathbf{k}^{(i)}(x)^T B^{-1}_{\epsilon,i}(\mathbf{m}^{(i)} - \mathbf{v}) \tag{38}$$

$$k_{u|\mathbf{v}}(x,y) = k_i(x,y) - \mathbf{k}^{(i)}(x)^T B^{-1}_{\epsilon,i}\mathbf{k}^{(i)}(y) \tag{39}$$

$$B_{\epsilon,i} := \epsilon^2 I + S\Sigma_i S^\dagger = \epsilon^2 I + C_{Y,i} \tag{40}$$

$$\mathbf{k}^{(i)}(x) := (k_i(x,y_1), \ldots, k_i(x,y_s))^T \tag{41}$$

where $k^{(i)}_{u|\mathbf{v}}$ is the covariance function associated with $\Sigma^{(i)}_{u|\mathbf{v}}$ and where the matrix $C_{Y,i} := S\Sigma_i S^\dagger \in \mathbb{R}^{s\times s}$ has pq-th entry $k_i(y_p, y_q)$. The specific sensor observations used in the experiments were obtained by simulating a trajectory from $\nu_\star$ evaluated at the locations $y_1, \ldots, y_s$.

Since we have the true posterior in an explicit form we can now demonstrate that the error bound for the full StatFEM posterior agrees with the error bound for linear quantities of interest from the posterior given in Theorem 4. We demonstrate this error bound for 4 different levels of sensor noise, $\epsilon = 0.00005, 0.0001, 0.01, 0.1$. These levels are chosen so that the lower values are comparable to the prior variances. We take $s = 10$

sensor readings equally spaced in the interval $[0.01, 0.99] \subset D$. For each level of sensor noise we again follow the argument outlined in Remark 4 and compute, for a range of sufficiently small h-values, an approximation of the Wasserstein distance between the two posteriors, and plot these results on a log-log scale. We take a reference grid of $N = 41$ equally spaced points in $[0, 1]$ to compare the covariances, and we take 28 h-values in $[0.025, 0.25]$. With these choices we obtain the plot shown in Fig. 2 below. We also present the estimates for the slopes and intercepts of the lines of best fit in Table 1.

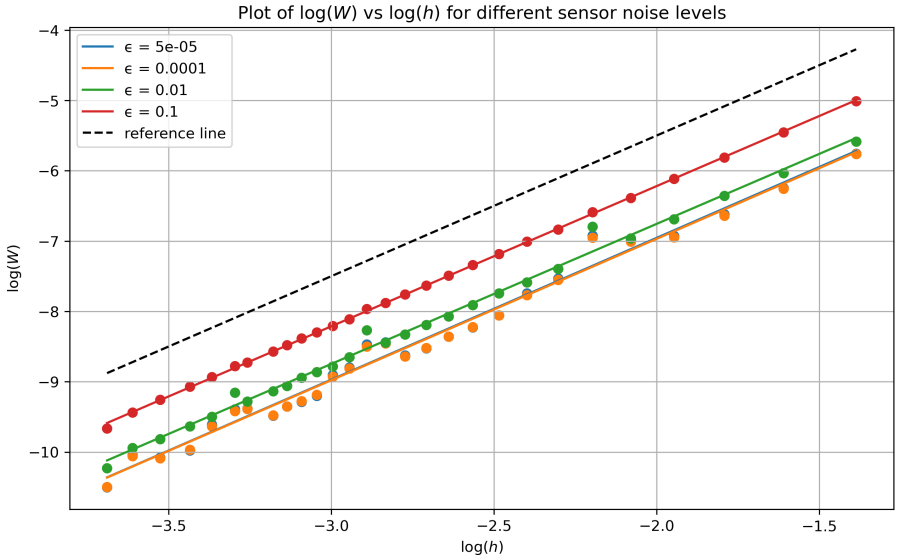

Figure 2: Log-log plot of Wasserstein distance against h for the posteriors in a 1-D example for varying levels of sensor noise. The reference line has a slope of 2. Notice how the best fit lines are all parallel to the reference line.

Table 1: Estimate of slopes and intercepts for the different levels of sensor noise ϵ. All of the slopes are around 2.

ϵ	slope	intercept
0.00005	2.0162	-2.9227
0.00010	2.0102	-2.9486
0.01000	1.9912	-2.7739
0.10000	1.9940	-2.2309

We can see from Fig. 2 and Table 1 that we obtain lines of best-fit which are all parallel to each other, each with a slope of around $p = 2$. The intercepts are slightly different for each level of sensor noise, as is to be expected since the constant in Theorem 4 depends upon ϵ. These results show that the error bound for the full posterior distributions is

also of order $p = 2$, suggesting that it is possible to extend Theorem 4 to the Wasserstein distance between the full posteriors. Proving this is left to future research.

4.2 Two-dimensional Poisson Equation

In this section we will present a numerical example involving the following two-dimensional Poisson equation:

$$\begin{aligned} -\Delta u(x) &= f(x) \qquad x \in D := [0,1]^2 \\ u(x) &= 0 \qquad x \in \partial D \end{aligned} \tag{42}$$

where the forcing f is distributed as,

$$f \sim \mathcal{GP}(\bar{f}, k_f) \tag{43}$$

with mean and covariance given by

$$\bar{f}(x) = 1 \tag{44}$$

$$k_f(x,y) = \sigma_f^2 \exp\left(-\frac{\|x-y\|^2}{2l_f^2}\right). \tag{45}$$

Again we took $\sigma_f = 0.1$ and $l_f = 0.4$. Note that the BVP Eq. (42) is an instance of the general problem Eq. (4) with $d = 2$, $D = [0,1]^2$, and $\kappa(x) \equiv 1$. For this problem we use the approach outlined in Remark 5 below to demonstrate the error bounds. We present the error estimates for the prior and posterior separately in the following sections.

4.2.1 Prior results for 2-D example

Following the notation of Theorem 3 we denote the StatFEM prior by ν_h. Since we do not have access to the true distributions here we will need an alternative approach to that of Remark 4. This approach is outlined in the remark, taken from [1], below:

Remark 5. When we do not have access to the true distributions we can proceed as follows. Again assuming that we have a rate of convergence, p, as given by Eq. (35), we can obtain an estimate as follows. First we utilise the triangle inequality to obtain,

$$W(\eta_h, \eta_{h/2}) \leq W(\eta_h, \eta_\star) + W(\eta_\star, \eta_{h/2}) \tag{46}$$

Together with Eq. (36) this yields,

$$W(\eta_h, \eta_{h/2}) = Ch^p + C(h/2)^p + \mathcal{O}(h^{p+1}) \tag{47}$$

Similarly we have,

$$W(\eta_{h/2}, \eta_{h/4}) = C(h/2)^p + C(h/4)^p + \mathcal{O}(h^{p+1}) \tag{48}$$

Dividing the two above equations yields,

$$\begin{aligned}\frac{W(\eta_h, \eta_{h/2})}{W(\eta_{h/2}, \eta_{h/4})} &= \frac{Ch^p + C(h/2)^p + \mathcal{O}(h^{p+1})}{C(h/2)^p + C(h/4)^p + \mathcal{O}(h^{p+1})} \\ &= \frac{1 - 2^{-p} + \mathcal{O}(h)}{2^{-p} - 2^{-2p} + \mathcal{O}(h)} \\ &= 2^p + \mathcal{O}(h) \end{aligned} \tag{49}$$

from which it follows that,

$$\mathrm{LR}(h) := \log_2 \frac{W(\eta_h, \eta_{h/2})}{W(\eta_{h/2}, \eta_{h/4})} = p + \mathcal{O}(h) \tag{50}$$

From the above equation we can see that we can obtain an estimate of the rate of convergence by computing, for a range of sufficiently small h-values, the base-2 logarithm of the ratio $W(\eta_h, \eta_{h/2})/W(\eta_{h/2}, \eta_{h/4})$ and seeing what these logarithms tend to as h gets very small. ♦

As outlined in Remark 5 above we will compute, for a range of sufficiently small h-values, the base-2 logarithm of the ratio $W(\nu_h, \nu_{h/2})/W(\nu_{h/2}, \nu_{h/4})$ and see what these logarithms tend to as h approaches 0. From the results of Theorem 3 we expect the logarithms to converge to 2.

We take a reference grid of $M = 41^2 = 1681$ equally spaced points in $[0, 1]^2$ to compare the covariances. We compute the logarithms for 59 h-values in the interval $[0.0275, 0.315]$. Note that these h-values are not equally spaced; instead they are arranged according to a refinement strategy which was utilised for efficient use of memory. With these choices we obtain the plot shown in Fig. 3 on the next page.

From this plot we can see that the logarithms seem to be approaching $p = 2$ as $h \to 0$, as our theory suggests. However, the results are somewhat oscillatory, which is to be expected for the approach outlined in Remark 5. Nevertheless the results seem to be oscillating around 2. To illustrate this more we smooth the above results by first discarding the results for larger h-values and then computing a cumulative average of the ratios before applying the base-2 logarithm. Note that this cumulative average is taken by starting with the results for large h first. We take our cutoff point to be $h = 0.15$. These smoothed results are shown in Fig. 4.

From Fig. 4 we can see that by discarding the values corresponding to $h > 0.15$ the base-2 logarithms of the rolling averages converge to a value slightly greater than 2. The final logarithm for these rolling averages is $p = 2.02$ (to 2 decimal places). Thus, we obtain results in close agreement with Theorem 3.

4.2.2 Posterior results for 2-D example

For this example we will consider the same specific case of the general Bayesian inverse problem which we chose in Section 4.1.2. That is, we will again take the observation operator S to be an evaluation operator. Since we do not have the true prior in an

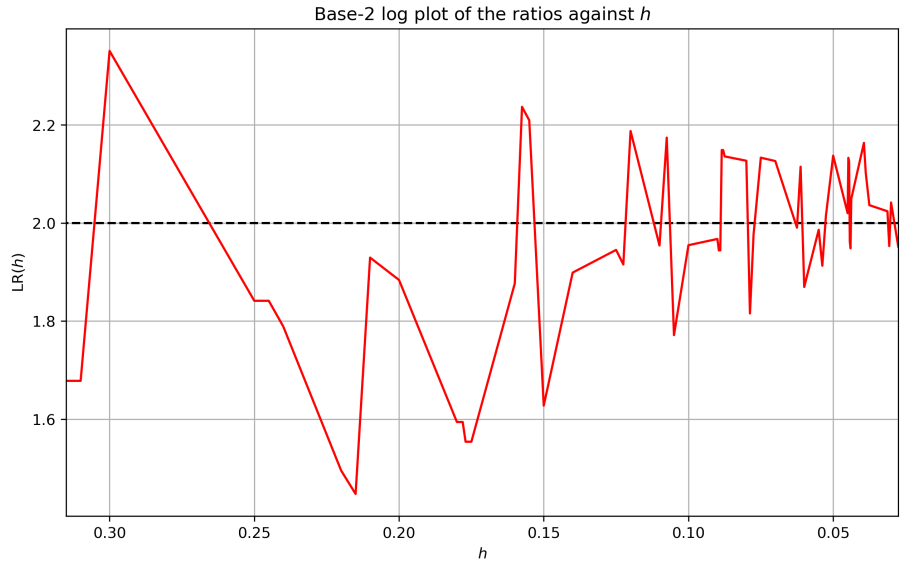

Figure 3: Plot of LR(h) against h, in the prior case, for our 2-D example.

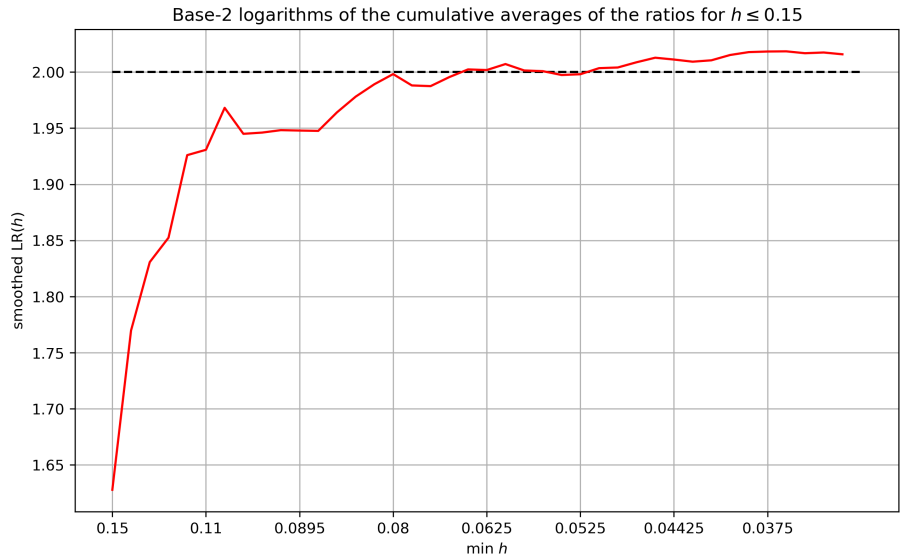

Figure 4: Plot of smoothed LR(h) for $h \leq 0.15$, in the prior case. The horizontal axis indicates the smallest h value taken in the cumulative averages.

explicit form, we also do not have the true posterior and as such we will utilise the argument in Remark 5 to demonstrate the StatFEM posterior error bound. To generate sensor readings, since we do not have access to the true prior, we instead simulated trajectories from the StatFEM prior with a very fine grid of mesh size $h = 1/120$.

We take a reference grid of $M = 41^2 = 1681$ equally spaced points in $[0, 1]^2$ to compare

the covariances. We set the sensor noise level to $\epsilon = 0.001$ and take $s = 25$ sensor readings equally spaced in $[0.01, 0.99]^2 \subset D$. The level of sensor noise is chosen to be comparable to the prior variances. We follow the notation of Theorem 4 and denote the StatFEM posterior by $\tilde{\nu}_h$. We compute the logarithms $\log_2 \left(W(\tilde{\nu}_h, \tilde{\nu}_{h/2}) / W(\tilde{\nu}_{h/2}, \tilde{\nu}_{h/4}) \right)$ for 53 h-values in the interval $[0.03125, 0.315]$, which are spread out according to the refinement strategy mentioned in Section 4.2.1. With these choices we obtain the plot shown in Fig. 5 below.

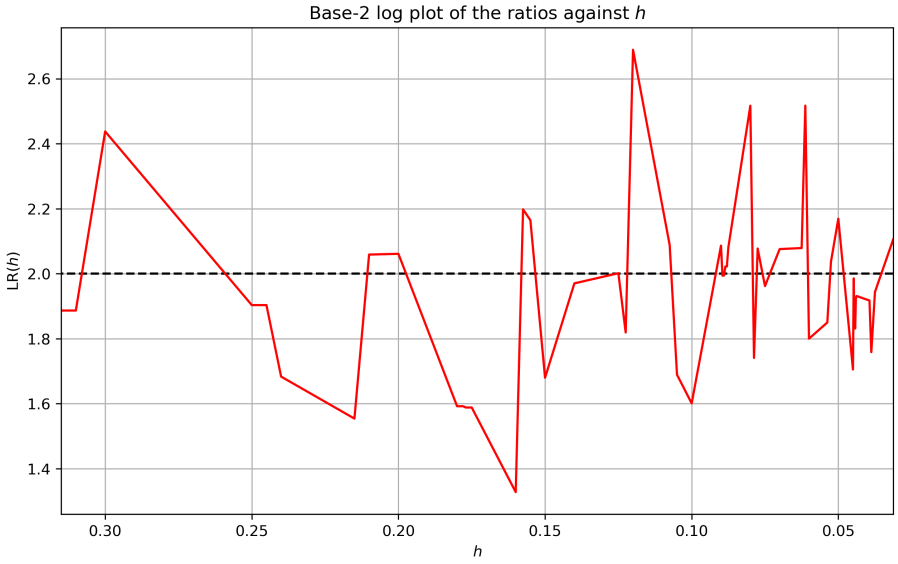

Figure 5: Plot of LR(h) against h, in the posterior case, for our 2-D example.

From this plot we can see that the logarithms seem to be approaching $p = 2$ as h gets small. However, just as in Section 4.2.1, the results are oscillatory but seem to be oscillating around $p = 2$. We will thus smooth the results as explained in Section 4.2.1. We again take the cutoff point to be $h = 0.15$. These smoothed results are shown in Fig. 6 on the next page. From this figure we can see that by discarding the values corresponding to $h > 0.15$ the base-2 logarithms of the rolling averages converge to a value slightly greater than 2. The final logarithm of these rolling averages is $p = 2.00$ (to 2 decimal places). Thus, just as in the 1D example we see results which suggest that it is possible to extend Theorem 4 to the case of the full posteriors.

4.3 Distribution of the maximum

In this section we will present a numerical experiment involving the same one-dimensional Poisson equation Eq. (27). The forcing f will follow the same distribution as given in Eq. (28), but we will adjust the kernel lengthscale to be $l_f = 0.01$ instead, as with a larger length-scale the maximum of the StatFEM prior and posterior were found to converge too quickly to demonstrate interesting behaviour. Since the solution, u, is random the

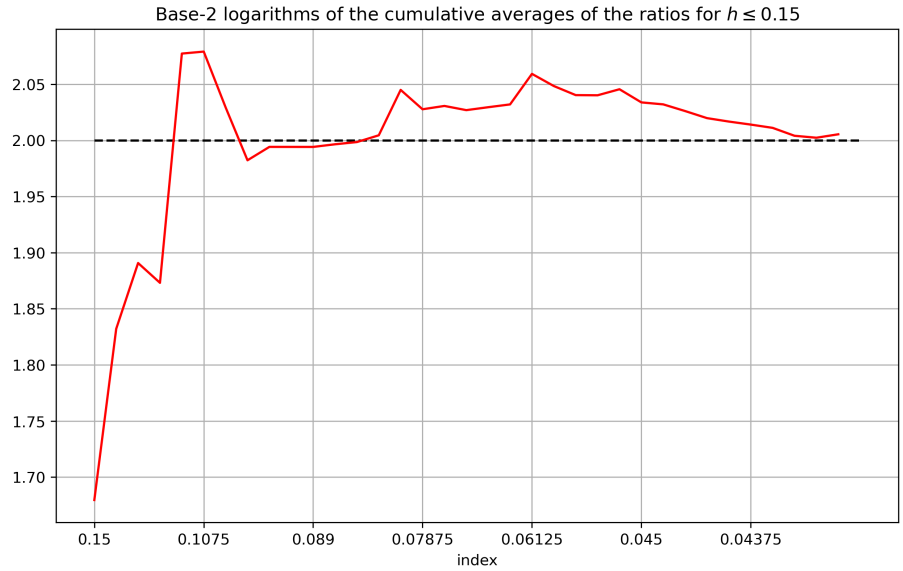

Figure 6: Plot of smoothed LR(h) for $h \leq 0.15$, in the posterior case. The horizontal axis indicates the smallest h value taken in the cumulative averages.

maximum, $\max_{x\in[0,1]} u(x)$, is a univariate random variable. Since taking the maximum is not a linear functional we have no guarantees that the distribution of the maximum will be Gaussian. More importantly our results from Theorem 4 will not necessarily hold for this example.

We will investigate the errors for the true and StatFEM prior/posterior distributions for the maximum via a Monte Carlo approach as we now outline in the following remark.

Remark 6. Let $\eta_\star, \eta_h$ denote the true and StatFEM prior (or posterior) for the maximum of u respectively. We are interested in investigating the rate of convergence of $W(\eta_\star, \eta_h)$ as $h \to 0$. This is done as follows: in both the prior and posterior case we will first fix a reference grid $\{\tilde{x}_i\}_{i=1}^N$ and obtain samples of trajectories of the solution on this grid from the true distribution. We then take the maximum values of these trajectories to obtain an (approximate) sample from the true distribution for $\max_{x\in[0,1]} u(x)$. For a range of h-values we will then simulate trajectories of the solution on the same reference grid from the StatFEM distribution and then take the maximum values of these to obtain an (approximate) sample for the StatFEM case. We will then compute an approximation of the Wasserstein distance $W(\eta_\star, \eta_h)$ by computing the Wasserstein distance between these two empirical distributions for each h-value by utilising the Python package `POT` [13]. We then investigate the rate of convergence as outlined previously in Remark 4. ♦

The results for the StatFEM priors and posteriors will be presented separately in the following sections.

4.4 Prior results for maximum example

As outlined in Remarks 4 and 6, we compute, for a range of sufficiently small h-values, a Monte Carlo approximation to the Wasserstein distance between the two priors for the maximum. We take a reference grid of $N = 100$ equally spaced points in $[0, 1]$ and 30 h-values in $[0.02, 0.25]$. We simulate 1000 trajectories from both priors to obtain approximate samples of the maximum. With these choices we obtain the plot shown in Fig. 7 below. From this plot we can see that the we indeed have convergence of the Wasserstein distance for this non-linear quantity of interest to 0, but at a different rate than that given in Theorem 3. The slope is estimated to be $p = 1.35$ (to 2 decimal places).

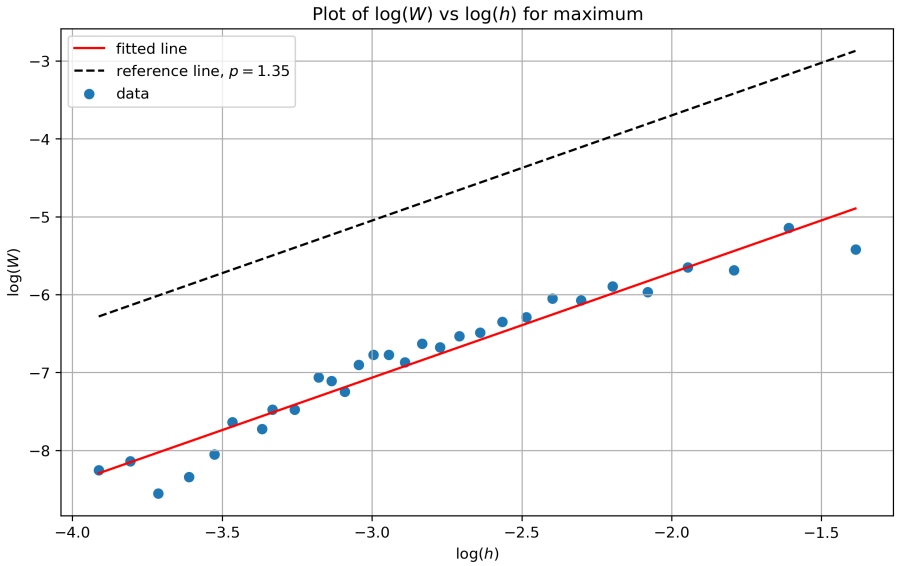

Figure 7: Log-log plot of Wasserstein distance against h for the priors for the maximum. The reference line has a slope of 1.35. The slope of the fitted line is estimated to be $p = 1.35$, in agreement visually with the reference line.

4.5 Posterior results for maximum example

For the posterior case we take a reference grid of $N = 41$ equally spaced points in $[0, 1]$ to simulate 1000 trajectories and 30 h-values in $[0.02, 0.25]$. We take $s = 10$ sensor readings equally spaced in the interval $[0.01, 0.99]$. This is repeated for 4 different levels of sensor noise, $\epsilon = 0.0001, 0.0005, 0.001, 0.01$, again chosen so that the lower noise levels are comparable to the prior variances. For each level of noise we follow the argument outlined in Remarks 4 and 6. With these choices we obtain the plot shown in Fig. 8 on the next page. We also present the estimates for the slopes and intercepts of the lines of best fit in Table 2.

From Fig. 8 and Table 2 we can see that for each level of sensor noise we do indeed have

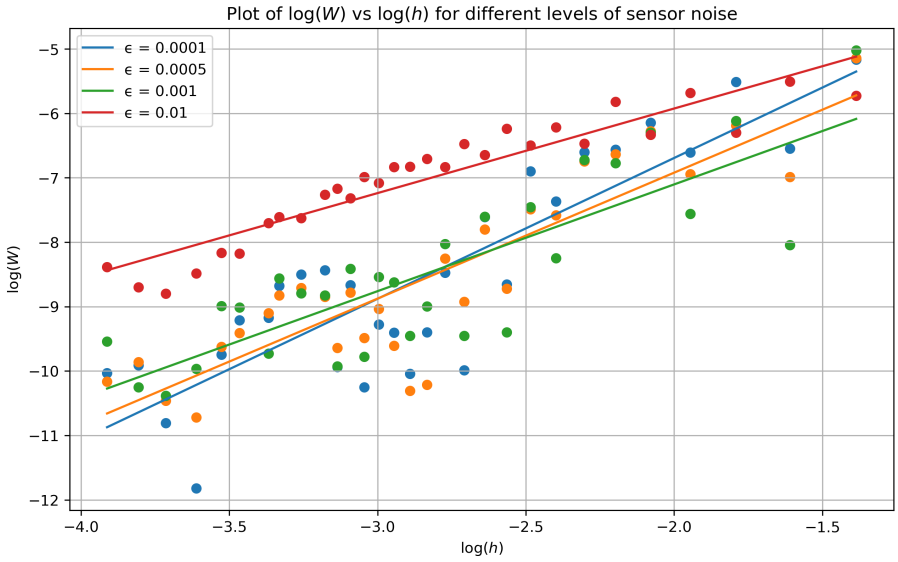

Figure 8: Log-log plot of Wasserstein distance against h for the posteriors for the maximum for different levels of sensor noise.

Table 2: Estimate of slopes and intercepts for the different levels of sensor noise ϵ.

ϵ	slope	intercept
0.00010	2.1862	-2.3203
0.00050	1.9552	-3.0104
0.00100	1.6573	-3.7885
0.01000	1.3131	-3.2989

convergence to 0 as h goes to 0. However, we observe that the rate is not always the same as that given in Theorem 4. From Table 2 it is particularly clear that as the sensor noise level decreases the rate of convergence increases. In particular, for $\epsilon = 0.0001, 0.0005$ we have rates around $p = 2$, similar to the case of linear quantities of interest. We hypothesise that this is because as the sensor noise decreases the posterior distribution concentrates more as the solution is better identified and this, combined with the fact that we take sensor readings close to the where the true prior mean Eq. (33) has a maximum, forces the maximum of the simulated trajectories to always be at the argmax of the prior mean in the exact case, i.e. at $x = 0.5$. Thus for very low levels of sensor noise taking the maximum of the posterior draws is almost identical to evaluating the solution at $x = 0.5$; such an evaluation is a linear quantity of interest and so one would expect the results from Theorem 4 to hold.

5 Conclusion

In this paper we have provided detailed error analysis for the StatFEM method first introduced in [14, 15] for the case of spatial elliptic BVPs. In particular, we have proven that the StatFEM prior converges, with respect to the Wasserstein-2 distance, to the true prior at a rate of $\mathcal{O}(h^2)$. We also showed that in the posterior case linear quantities of interest are also controlled at a rate of $\mathcal{O}(h^2)$. In both settings, the choice of the Wasserstein distance provides a convenient metric in which to quantify the error introduced through discretisation. Numerical experiments demonstrating the theoretical results on standard FEM test problems were then presented. These demonstrated the rates for the prior theory, while also showcasing that it may be possible to extend the posterior results to the full distribution as opposed to just linear quantities of interest. An example involving a non-linear quantity of interest was also presented, showcasing an example which lies out of the remit of our theory.

Several possible avenues for future work present themselves. The first would be to prove error bounds for the full posterior distributions, extending Theorem 4. Another avenue would be to provide similar error analysis for StatFEM in the case of time-dependent problems. It would also be interesting to see if similar error bounds can be proven for distributions utilising approximations other than FEM. Generalising the results to utilise Wasserstein-p distance, for $p > 2$, would also be an interesting goal, as this will allow one to have even more control over other aspects of the distribution such as quantiles and extrema, which is especially important for risk-assessment applications.

References

[1] Verifying numerical convergence rates. Technical report, KTH. https://www.csc.kth.se/utbildning/kth/kurser/DN2255/ndiff13/ConvRate.pdf.

[2] M. Aldosary, J. Wang, and C. Li. Structural reliability and stochastic finite element methods. *Engineering Computations*, 2018.

[3] V. I. Bogachev. *Gaussian measures*. Number 62. American Mathematical Soc., 1998.

[4] O. A. Chkrebtii, D. A. Campbell, B. Calderhead, M. A. Girolami, et al. Bayesian solution uncertainty quantification for differential equations. *Bayesian Analysis*, 11 (4):1239–1267, 2016.

[5] J. Cockayne, C. Oates, T. Sullivan, and M. Girolami. Probabilistic numerical methods for partial differential equations and bayesian inverse problems. *arXiv preprint arXiv:1605.07811*, 2016.

[6] J. Cockayne, C. J. Oates, T. J. Sullivan, and M. Girolami. Bayesian probabilistic numerical methods. *SIAM Review*, 61(4):756–789, 2019.

[7] P. R. Conrad, M. Girolami, S. Särkkä, A. Stuart, and K. Zygalakis. Statistical analysis of differential equations: introducing probability measures on numerical solutions. *Statistics and Computing*, 27(4):1065–1082, 2017.

[8] S. L. Cotter, M. Dashti, J. C. Robinson, and A. M. Stuart. Bayesian inverse problems for functions and applications to fluid mechanics. *Inverse problems*, 25(11): 115008, 2009.

[9] J. Cuesta-Albertos, C. Matrán-Bea, and A. Tuero-Diaz. On lower bounds for the l2-wasserstein metric in a hilbert space. *Journal of Theoretical Probability*, 9(2): 263–283, 1996.

[10] G. Da Prato and J. Zabczyk. *Stochastic equations in infinite dimensions*. Cambridge university press, 2014.

[11] D. Dowson and B. Landau. The fréchet distance between multivariate normal distributions. *Journal of multivariate analysis*, 12(3):450–455, 1982.

[12] L. C. Evans. *Partial differential equations*. American Mathematical Society, Providence, R.I., 2010. ISBN 9780821849743 0821849743.

[13] R. Flamary, N. Courty, A. Gramfort, M. Z. Alaya, A. Boisbunon, S. Chambon, L. Chapel, A. Corenflos, K. Fatras, N. Fournier, L. Gautheron, N. T. Gayraud, H. Janati, A. Rakotomamonjy, I. Redko, A. Rolet, A. Schutz, V. Seguy, D. J. Sutherland, R. Tavenard, A. Tong, and T. Vayer. Pot: Python optimal transport. *Journal of Machine Learning Research*, 22(78):1–8, 2021. URL http://jmlr.org/papers/v22/20-451.html.

[14] M. Girolami, A. Gregory, G. Yin, and F. Cirak. The statistical finite element method. *arXiv preprint arXiv:1905.06391*, 2019.

[15] M. Girolami, E. Febrianto, G. Yin, and F. Cirak. The statistical finite element method (statFEM) for coherent synthesis of observation data and model predictions. *Computer Methods in Applied Mechanics and Engineering*, 375:113533, Mar. 2021. doi: 10.1016/j.cma.2020.113533. URL https://doi.org/10.1016/j.cma.2020.113533.

[16] P. Grisvard. *Elliptic problems in nonsmooth domains*. SIAM, 2011.

[17] P. Hennig, M. A. Osborne, and M. Girolami. Probabilistic numerics and uncertainty in computations. *Proceedings of the Royal Society A: Mathematical, Physical and Engineering Sciences*, 471(2179):20150142, 2015.

[18] S. Larsson and V. Thomée. *Partial differential equations with numerical methods*, volume 45. Springer Science & Business Media, 2008.

[19] F. Lindgren, H. Rue, and J. Lindström. An explicit link between gaussian fields and gaussian markov random fields: the stochastic partial differential equation approach. *Journal of the Royal Statistical Society: Series B (Statistical Methodology)*, 73(4):423–498, 2011.

[20] G. J. Lord, C. E. Powell, and T. Shardlow. *An introduction to computational stochastic PDEs*, volume 50. Cambridge University Press, 2014.

[21] S. Martino and A. Riebler. Integrated nested laplace approximations (inla). *Wiley StatsRef: Statistics Reference Online*, pages 1–19, 2014.

[22] V. Masarotto, V. M. Panaretos, and Y. Zemel. Procrustes metrics on covariance operators and optimal transportation of gaussian processes. *Sankhya A*, 81(1):172–213, 2019.

[23] H. G. Matthies, C. E. Brenner, C. G. Bucher, and C. Guedes Soares. Uncertainties in probabilistic numerical analysis of structures and solids-stochastic finite elements. *Structural Safety*, 19(3):283–336, 1997. ISSN 0167-4730. doi: https://doi.org/10.1016/S0167-4730(97)00013-1. URL https://www.sciencedirect.com/science/article/pii/S0167473097000131. Devoted to the work of the Joint Committee on Structural Safety.

[24] I. Olkin and F. Pukelsheim. The distance between two random vectors with given dispersion matrices. *Linear Algebra and its Applications*, 48:257–263, 1982.

[25] H. Owhadi. Bayesian numerical homogenization. *Multiscale Modeling & Simulation*, 13(3):812–828, 2015.

[26] C. E. Rasmussen. *Gaussian processes for machine learning*. MIT Press, 2006.

[27] M. Scheuerer. Regularity of the sample paths of a general second order random field. *Stochastic Processes and their Applications*, 120(10):1879–1897, 2010.

[28] F. Sigrist, H. R. Künsch, and W. A. Stahel. Stochastic partial differential equation based modelling of large space–time data sets. *Journal of the Royal Statistical Society: Series B: Statistical Methodology*, pages 3–33, 2015.

[29] G. Stefanou. The stochastic finite element method: Past, present and future. *Computer Methods in Applied Mechanics and Engineering*, 198(9):1031–1051, 2009. ISSN 0045-7825. doi: https://doi.org/10.1016/j.cma.2008.11.007. URL https://www.sciencedirect.com/science/article/pii/S0045782508004118.

[30] G. Strang and G. J. Fix. An analysis of the finite element method. *Journal of Applied Mathematics and Mechanics*, 1973.

[31] A. M. Stuart. Inverse problems: a bayesian perspective. *Acta numerica*, 19:451–559, 2010.

[32] B. Sudret and A. Der Kiureghian. *Stochastic finite element methods and reliability: a state-of-the-art report*. Department of Civil and Environmental Engineering, University of California ..., 2000.

[33] F. Tronarp, H. Kersting, S. Särkkä, and P. Hennig. Probabilistic solutions to ordinary differential equations as nonlinear bayesian filtering: a new perspective. *Statistics and Computing*, 29(6):1297–1315, 2019.

[34] D. Xiu. *Numerical methods for stochastic computations: a spectral method approach*. Princeton university press, 2010.

[35] Z. Zhang and G. Karniadakis. *Numerical methods for stochastic partial differential equations with white noise*. Springer, 2017.

Supplementary Material

For: Theoretical Guarantees for the Statistical Finite Element Method

Yanni Papandreou* Jon Cockayne † Mark Girolami ‡
Andrew B. Duncan§

November 15, 2021

S1 Implementation Details for Experiments

In this section we present three remarks which give further details on the implementation of the experiments in Section 4.

Remark 1. In both the statistical finite element method (StatFEM) prior and posterior the $n_u \times n_u$ matrix $K_{\mathcal{F}_h} = \mathcal{F}_h K \mathcal{F}_h^\dagger$ appears. This is the covariance matrix for the random load vector $\mathbf{f} = \mathcal{F}_h f$. The ij-*th* element of this covariance matrix is given by:

$$(K_{\mathcal{F}_h})_{ij} = \int_D \int_D \phi_i(x) k_f(x, y) \phi_j(y) \mathrm{d}x \mathrm{d}y. \tag{S1}$$

For a covariance function k_f which is globally supported, the covariance matrix, $K_{\mathcal{F}_h}$, is dense as can be seen from expression Eq. (S1) above. As such, it can be very difficult to efficiently compute and assemble the entries of this matrix. We thus employ an approximation of this matrix, by interpolating the covariance function k_f with the finite element basis functions, as suggested by [S2]. I.e., denoting the non-boundary nodes of the FE triangulation by $\{x_i\}_{i=1}^{n_u}$, we approximate k_f by,

$$k_f(x, y) \approx \sum_{k,l=1}^{n_u} \phi_k(x) k_f(x_k, x_l) \phi_l(y) \tag{S2}$$

*Imperial College London (john.papandreou18@imperial.ac.uk)
†The Alan Turing Institute (jcockayne@turing.ac.uk)
‡The Alan Turing Institute and University of Cambridge (mag92@cam.ac.uk)
§Imperial College London and The Alan Turing Institute (a.duncan@imperial.ac.uk)

Using this interpolation of k_f we can approximate the entries of $K_{\mathcal{F}_h}$ by,

$$\begin{aligned}(K_{\mathcal{F}_h})_{ij} &\approx \sum_{k,l=1}^{n_u} k_f(x_k, x_l) \int_D \int_D \phi_i(x)\phi_k(x)\phi_j(y)\phi_l(y)\mathrm{d}x\mathrm{d}y \\ &= \sum_{k,l=1}^{n_u} k_f(x_k, x_l) \int_D \phi_i(x)\phi_k(x)\mathrm{d}x \int_D \phi_j(y)\phi_l(y)\mathrm{d}y \\ &= \sum_{k,l=1}^{n_u} k_f(x_k, x_l) M_{ik} M_{jl} \\ &= (M C_f M^T)_{ij}\end{aligned}$$

i.e. we can approximate:

$$K_{\mathcal{F}_h} \approx M C_f M^T \tag{S3}$$

where $C_f \in \mathbb{R}^{n_u \times n_u}$ is the covariance matrix corresponding to evaluating k_f on the non-boundary nodes, $\{x_i\}_{i=1}^{n_u}$, of the Finite Element Method (FEM) triangulation, and M is the mass matrix introduced in Section 2.1. This approximation will improve as h gets smaller. ⧫

Remark 2. Since all of the true and StatFEM priors and posteriors are Gaussian measures, and since we are interested in demonstrating a bound on the error between the respective priors and posteriors for the Wasserstein-2 distance the expression Eq. (3) will be useful. Focussing on the covariance contribution in Eq. (3), note that this is difficult to compute explicitly for the measures in this paper. For two Gaussian processes (GPs) $\nu_i \sim \mathcal{N}(0, \Sigma_i)$, $i \in \{1, 2\}$ we approximate the covariance contribution by fixing a fine reference grid $\{\tilde{x}_i\}_{i=1}^N$, computing the covariance matrices, $C_i = \{k_i(\tilde{x}_k, \tilde{x}_l)\}_{k,l=1}^N$, corresponding to the covariance operators, Σ_i, evaluated on this reference grid, where k_i is the covariance function associated with Σ_i respectively, and finally approximating the Wasserstein distance as follows:

$$\begin{aligned}W^2(\mathcal{N}(0, \Sigma_1), \mathcal{N}(0, \Sigma_2)) &= \mathrm{tr}(\Sigma_1) + \mathrm{tr}(\Sigma_2) - 2\,\mathrm{tr}\sqrt{\Sigma_1^{1/2}\Sigma_2\Sigma_1^{1/2}} \\ &\approx \mathrm{tr}(C_1) + \mathrm{tr}(C_2) - 2\,\mathrm{tr}\sqrt{C_1^{1/2}C_2C_1^{1/2}}.\end{aligned} \tag{S4}$$

⧫

Remark 3. Let $m_\star, m_h$ denote the means of the true and StatFEM prior (or posterior) respectively. The mean contribution to the Wasserstein-2 distance is $\|m_\star - m_h\|_{L^2(D)}$. This contribution can be easily approximated by utilising a modern FEM package such as `FEniCS`, which we use in this paper. ⧫

S2 Proofs

In this section the proofs of the main theoretical results are presented.

Proof of Proposition 1. This follows trivially from the fact that the approximate solution operator is a linear map together with the well known transformation results of a Gaussian measure by linear maps. ■

Proof of Proposition 2. We first note that so far we have assumed that the priors $u \sim \nu_i = \mathcal{N}(m_i, \Sigma_i)$ are Gaussian measures on $L^2(D)$. However, both priors are actually supported on subspaces $V_i \subseteq L^2(D)$. For the purposes of the proof we will be viewing the priors as measures on the respective subspaces V_i. We will then trivially extend the resulting posteriors onto all of $L^2(D)$. When viewed as Gaussian measures on V_i the covariance operators Σ_i are both positive definite.

In order to obtain the posterior $\widetilde{\nu}_i$ we will first derive the joint distribution of $(u, \mathbf{v})^T$ when the prior on u is ν_i. Since the observational noise $\boldsymbol{\xi}$ is independent of $\mathbf{u}$ we have that the joint distribution of $(u, \boldsymbol{\xi})^T$ is:

$$\begin{pmatrix} u \\ \boldsymbol{\xi} \end{pmatrix} \sim \mathcal{N}\left(\begin{pmatrix} m_i \\ \mathbf{0} \end{pmatrix}, \begin{pmatrix} \Sigma_i & 0 \\ 0 & \epsilon^2 I \end{pmatrix} \right). \tag{S5}$$

Using the definition Eq. (20) of $\mathbf{v}$ we now note that $(u, \mathbf{v})^T$ can be expressed as:

$$\begin{pmatrix} u \\ \mathbf{v} \end{pmatrix} = \begin{pmatrix} I & 0 \\ S & I \end{pmatrix} \begin{pmatrix} u \\ \boldsymbol{\xi} \end{pmatrix} \tag{S6}$$

Since this is a linear transformation of $(u, \boldsymbol{\xi})^T$ we have that the joint distribution of $(u, \mathbf{v})^T$ is given by:

$$\begin{pmatrix} u \\ \mathbf{v} \end{pmatrix} \sim \mathcal{N}\left(\begin{pmatrix} m_i \\ Sm_i \end{pmatrix}, \begin{pmatrix} \Sigma_i & \Sigma_i S^\dagger \\ S\Sigma_i & \epsilon^2 I + S\Sigma_i S^\dagger \end{pmatrix} \right) \tag{S7}$$

From this it is simply a matter of conditioning to obtain the posterior distribution of $u|\mathbf{v}$ specified by Eqs. (23) and (24). This conditioning step is justified under the following result taken from [S4, see Theorem 6.20].

Theorem 1 (Conditioning of Gaussian measures)**.** *Let $\mathcal{H} = \mathcal{H}_1 \oplus \mathcal{H}_2$ be a separable Hilbert space with projectors $\Pi_i : \mathcal{H} \to \mathcal{H}_i$. Let $(x_1, x_2) \in \mathcal{H}_1 \oplus \mathcal{H}_2$ be an $\mathcal{H}$-valued Gaussian random variable with mean $m = (m_1, m_2)$ and positive definite covariance operator $\mathcal{C}$. Define*

$$C_{ij} = \mathbb{E}(x_i - m_i) \otimes (x_j - m_j) \tag{S8}$$

Then the conditional distribution of x_1 given x_2 is Gaussian with mean

$$m' = m_1 + \mathcal{C}_{12}\mathcal{C}_{22}^{-1}(x_2 - m_2) \tag{S9}$$

and covariance operator

$$\mathcal{C}' = \mathcal{C}_{11} - \mathcal{C}_{12}C_{22}^{-1}\mathcal{C}_{21} \tag{S10}$$

♦

This theorem is applied in our case with $\mathcal{H}_1 = V_i$ and $\mathcal{H}_2 = \mathbb{R}^s$. The corresponding covariance operator $\mathcal{C}$ is given by the operator in Eq. (S7). The only thing which remains to show is that this covariance operator is positive definite. To that end, note that we can rewrite this operator as:

$$\begin{aligned}\mathcal{C} = \begin{pmatrix} \Sigma_i & \Sigma_i S^\dagger \\ S\Sigma_i & \epsilon^2 I + S\Sigma_i S^\dagger \end{pmatrix} &= \begin{pmatrix} \Sigma_i & \Sigma_i S^\dagger \\ S\Sigma_i & S\Sigma_i S^\dagger \end{pmatrix} + \begin{pmatrix} 0 & 0 \\ 0 & \epsilon^2 I \end{pmatrix} \\ &= \underbrace{\begin{pmatrix} I \\ S \end{pmatrix} \Sigma_i \begin{pmatrix} I & S^\dagger \end{pmatrix}}_{(a)} + \underbrace{\begin{pmatrix} 0 & 0 \\ 0 & \epsilon^2 I \end{pmatrix}}_{(b)} \end{aligned} \tag{S11}$$

Written in this form it is clear that $\mathcal{C}$ is positive definite. This is because operator (a) above is positive definite while operator (b) is positive semi-definite. Positive definiteness of (a) follows from the positive definiteness of Σ_i together with the fact that S satisfies Assumption 4. ■

Before we provide proofs for Theorems 3 and 4 we first present several lemmas which will be required in the proofs. The first of these is a simple corollary to Theorem 2 which places a bound on the operator norm of the difference of the solution operators $\mathcal{L}^{-1}$ and $\hat{L}_h^{-1}$.

Lemma 1. Under the assumptions of Theorem 2 we have the following bound for sufficiently small h:

$$\|\mathcal{L}^{-1} - \hat{L}_h^{-1}\|_{L^2} \leq Ch^2 \tag{S12}$$

where we have used the notation $\|\cdot\|_{L^2}$ to denote the operator norm for operators from $L^2(D) \to L^2(D)$. ♦

Proof of Lemma 1. This bound on the operator norm of $\mathcal{L}^{-1} - \hat{L}_h^{-1}$ follows from noting that the error bound Eq. (14) given in Theorem 2 can be re-expressed as:

$$\|\mathcal{L}^{-1} f - \hat{L}_h^{-1} f\|_{L^2(D)} = \|(\mathcal{L}^{-1} - \hat{L}_h^{-1}) f\|_{L^2(D)} \leq Ch^2 \|f\|_{L^2(D)}$$

Since the above inequality holds for all $f \in L^2(D)$ we deduce that Eq. (S12) holds as required. ■

The next result we will need is a bound on the Wasserstein distance found in [S1, see Lemma S2]. We quote this lemma below:

Lemma 2. Let $\mu_1 = \mathcal{N}(a_1, C_1)$ and $\mu_2 = \mathcal{N}(a_2, C_2)$ each be Gaussian measures on a Hilbert space $\mathcal{H}$. Let S_1, S_2 each be square roots of C_1, C_2 such that $C_1 = S_1^\dagger S_1$ and $C_2 = S_2^\dagger S_2$. Then we have that,

$$W^2(\mu_1, \mu_2) \leq \|a_1 - a_2\|_{\mathcal{H}}^2 + \|S_1 - S_2\|_{\text{HS}}^2 \tag{S13}$$

♦

Remark 4. Lemma 2 above utilises the connection between the Wasserstein distance between Gaussian measures and the Procrustes Metric on the respective covariance operators mentioned above. ♦

We are now in a position to prove Theorems 3 and 4. We start by proving Theorem 3.

Proof of Theorem 3. Both of the priors $\nu_\star, \nu_h$ are Gaussian measures on the Hilbert space $L^2(D)$. Further, noting that K is a covariance operator, we have that it possesses a symmetric square root $K^{1/2}$, i.e. we have $K = K^{1/2}K^{1/2}$ and $(K^{1/2})^\dagger = K^{1/2}$. Using this fact, we see that we can express the covariance operators of the priors as follows:

$$\begin{aligned}\Sigma_\star &= \mathcal{L}^{-1}K\mathcal{L}^{-\dagger} \\ &= \mathcal{L}^{-1}K^{1/2}K^{1/2}\mathcal{L}^{-\dagger} \\ &= (K^{1/2}\mathcal{L}^{-\dagger})^\dagger(K^{1/2}\mathcal{L}^{-\dagger}) = S_\star^\dagger S_\star \qquad \text{(S14)} \\ \Sigma_h &= \hat{L}_h^{-1}K\hat{L}_h^{-\dagger} \\ &= \hat{L}_h^{-1}K^{1/2}K^{1/2}\hat{L}_h^{-\dagger} \\ &= (K^{1/2}\hat{L}_h^{-\dagger})^\dagger(K^{1/2}\hat{L}_h^{-\dagger}) = S_h^\dagger S_h \qquad \text{(S15)}\end{aligned}$$

where $S_\star := K^{1/2}\mathcal{L}^{-\dagger}$ and $S_h := K^{1/2}\hat{L}_h^{-\dagger}$. Thus, our priors $\nu_\star, \nu_h$ satisfy the assumptions of Lemma 2 and so utilising this lemma we obtain the following bound on the Wasserstein distance:

$$W^2(\nu_\star, \nu_h) \leq \|m_\star - m_h\|_{L^2(D)}^2 + \|S_\star - S_h\|_{\text{HS}}^2 \qquad \text{(S16)}$$

We now proceed to bound each of the terms in Eq. (S16). Starting with the first term we have, for sufficiently small h, the following:

$$\|m_\star - m_h\|_{L^2(D)} = \|\mathcal{L}^{-1}\bar{f} - \hat{L}_h^{-1}\bar{f}\|_{L^2(D)} \leq Ch^2\|\bar{f}\|_{L^2(D)} \qquad \text{(S17)}$$

where we have utilised the error bound from Theorem 2, which holds since $\bar{f} \in L^2(D)$ and since all of the Assumptions 1 to 3 hold. For the second term in Eq. (S16) we have:

$$\begin{aligned}\|S_\star - S_h\|_{\text{HS}} &= \|K^{1/2}\mathcal{L}^{-\dagger} - K^{1/2}\hat{L}_h^{-\dagger}\|_{\text{HS}} \qquad \text{(S18)} \\ &= \|K^{1/2}(\mathcal{L}^{-\dagger} - \hat{L}_h^{-\dagger})\|_{\text{HS}} \qquad \text{(S19)} \\ &\leq \|K^{1/2}\|_{HS}\|\mathcal{L}^{-\dagger} - \hat{L}_h^{-\dagger}\|_{L^2} \qquad \text{(S20)} \\ &= \|K^{1/2}\|_{\text{HS}}\|\mathcal{L}^{-1} - \hat{L}_h^{-1}\|_{L^2} \qquad \text{(S21)} \\ &\leq Ch^2\|K^{1/2}\|_{\text{HS}} \qquad \text{(S22)}\end{aligned}$$

We have utilised several facts in the above which we now detail. In going from Eq. (S19) to Eq. (S20) we have utilised the facts that $\mathcal{L}^{-1} - \hat{L}_h^{-1}$, and hence its adjoint $\mathcal{L}^{-\dagger} - \hat{L}_h^{-\dagger}$, is a bounded operator and that $K^{1/2}$ is Hilbert-Schmidt. This second fact follows from the facts that K and $K^{1/2}$ are symmetric and that K is positive and trace-class and computing $\|K^{1/2}\|_{\text{HS}} = \text{tr}(K^{1/2}K^{1/2})^{1/2} = \text{tr}(K)^{1/2} = \text{tr}((K^2)^{1/2})^{1/2} = \|K\|_{\text{tr}}^{1/2} < \infty$. Finally, in going from Eq. (S21) to Eq. (S22) we used the bound Eq. (S12) from Lemma 1.

We can now combine the bounds on these two terms to obtain for sufficiently small h, the following:

$$W^2(\nu_\star, \nu_h) \leq C^2 h^4 \|\bar{f}\|^2_{L^2(D)} + C^2 h^4 \|K^{1/2}\|^2_{\mathrm{HS}} \tag{S23}$$

$$= C^2 h^4 \left(\|\bar{f}\|^2_{L^2(D)} + \|K^{1/2}\|^2_{\mathrm{HS}} \right) \tag{S24}$$

which implies,

$$W(\nu_\star, \nu_h) \leq C \sqrt{\|\bar{f}\|^2_{L^2(D)} + \|K^{1/2}\|^2_{\mathrm{HS}}} h^2 = \gamma h^2 \tag{S25}$$

where $\gamma := C\sqrt{\|\bar{f}\|^2_{L^2(D)} + \|K^{1/2}\|^2_{\mathrm{HS}}} > 0$ is a positive constant, independent of h, as required. ■

We now prove Theorem 4.

Proof of Theorem 4. Since both of the posteriors $\tilde{\nu}_\star, \tilde{\nu}_h$ are Gaussians we have that $\ell\tilde{\nu}_\star \sim \mathcal{N}\left(\ell m^{(\star)}_{u|\mathbf{v}}, \ell\Sigma^{(\star)}_{u|\mathbf{v}}\ell^\dagger\right)$ and $\ell\tilde{\nu}_h \sim \mathcal{N}\left(\ell m^{(h)}_{u|\mathbf{v}}, \ell\Sigma^{(h)}_{u|\mathbf{v}}\ell^\dagger\right)$ are univariate Gaussians. Thus, we have via Eq. (3),

$$W^2(\ell\tilde{\nu}_\star, \ell\tilde{\nu}_h) = \left|\ell m^{(\star)}_{u|\mathbf{v}} - \ell m^{(h)}_{u|\mathbf{v}}\right|^2 + \left|\sqrt{\ell\Sigma^{(\star)}_{u|\mathbf{v}}\ell^\dagger} - \sqrt{\ell\Sigma^{(h)}_{u|\mathbf{v}}\ell^\dagger}\right|^2. \tag{S26}$$

We proceed to bound the two terms in the equation above. The following remark will be very useful throughout this proof.

Remark 5. Let $(\mathcal{X}, \|\cdot\|)$ be a normed vector space. Let $a, a_h \in \mathcal{X}$, where a_h depends on some discretisation parameter h. Suppose there are constants $\widetilde{M}, p > 0$ such that we have $\|a - a_h\| \leq \widetilde{M}h^p + \mathcal{O}(h^{p+1})$ as $h \to 0$. Then we can bound $\|a_h\|$ as follows:

$$\begin{aligned}
\|a_h\| &= \|a + (a_h - a)\| \\
&\leq \|a\| + \|a_h - a\| \\
&\leq \|a\| + \widetilde{M}h^p + \mathcal{O}(h^{p+1}) && \text{(S27)} \\
&\leq \|a\| + \mathcal{O}(h^p). && \text{(S28)}
\end{aligned}$$

Both of the forms Eq. (S27) and Eq. (S28) will be useful in what follows. ♦

It will be helpful to first derive a bound on $\|\Sigma_\star - \Sigma_h\|_{L^2}$. We proceed as follows:

$$\begin{aligned}
\|\Sigma_\star - \Sigma_h\|_{L^2} &= \|\mathcal{L}^{-1}K\mathcal{L}^{-\dagger} - \hat{L}_h^{-1}K\hat{L}_h^{-\dagger}\|_{L^2} \\
&\leq \|\mathcal{L}^{-1}K(\mathcal{L}^{-1} - \hat{L}_h^{-1})^\dagger\|_{L^2} + \|(\mathcal{L}^{-1} - \hat{L}_h^{-1})K\hat{L}_h^{-\dagger}\|_{L^2} \\
&\leq \|\mathcal{L}^{-1}\|_{L^2}\|K\|_{L^2}\|(\mathcal{L}^{-1} - \hat{L}_h^{-1})^\dagger\|_{L^2} + \|\mathcal{L}^{-1} - \hat{L}_h^{-1}\|_{L^2}\|K\|_{L^2}\|\hat{L}_h^{-\dagger}\|_{L^2} \\
&= (\|\mathcal{L}^{-1}\|_{L^2} + \underbrace{\|\hat{L}_h^{-1}\|_{L^2}}_{(a)})\|K\|_{L^2}\underbrace{\|\mathcal{L}^{-1} - \hat{L}_h^{-1}\|_{L^2}}_{(b)} \\
&\leq (2\|\mathcal{L}^{-1}\|_{L^2} + Ch^2)\|K\|_{L^2}Ch^2 \\
&\leq C_1 h^2 + \mathcal{O}(h^4) && \text{(S29)}
\end{aligned}$$

where $C_1 := 2\|\mathcal{L}^{-1}\|_{L^2}\|K\|_{L^2}C > 0$ is a constant independent of h. Note we have utilised Remark 5 to bound (a) and Lemma 1 to bound (b). We have also made use of the fact that $\|L\|_{\mathcal{X}\to\mathcal{Y}} = \|L^\dagger\|_{\mathcal{Y}\to\mathcal{X}}$ for a bounded linear operator between two Hilbert spaces. With this result we can now begin to bound the two terms in Eq. (S26). Starting with the mean term we have,

$$\begin{aligned}\left|\ell m^{(\star)}_{u|\mathbf{v}} - \ell m^{(h)}_{u|\mathbf{v}}\right| &= \left|\ell(m^{(\star)}_{u|\mathbf{v}} - m^{(h)}_{u|\mathbf{v}})\right| \\ &\leq \|\ell\|_{L^2(D)\to\mathbb{R}}\|m^{(\star)}_{u|\mathbf{v}} - m^{(h)}_{u|\mathbf{v}}\|_{L^2(D)}.\end{aligned}$$

Using the definitions of the posterior means we can bound,

$$\begin{aligned}\|m^{(\star)}_{u|\mathbf{v}} - m^{(h)}_{u|\mathbf{v}}\|_{L^2(D)} &= \|m_\star - m_h + \Sigma_\star S^\dagger B^{-1}_{\epsilon,\star}(\mathbf{v} - Sm_\star) - \Sigma_h S^\dagger B^{-1}_{\epsilon,h}(\mathbf{v} - Sm_h)\|_{L^2(D)} \\ &\leq \underbrace{\|m_\star - m_h\|_{L^2(D)}}_{(c)} + \underbrace{\|\Sigma_\star S^\dagger B^{-1}_{\epsilon,\star} - \Sigma_h S^\dagger B^{-1}_{\epsilon,h}\|_{\mathbb{R}^s\to L^2(D)}}_{(d)}\|\mathbf{v}\| \\ &\quad + \underbrace{\|\Sigma_\star S^\dagger B^{-1}_{\epsilon,\star} Sm_\star - \Sigma_h S^\dagger B^{-1}_{\epsilon,h} Sm_h\|_{L^2(D)}}_{(e)} \qquad \text{(S30)}\end{aligned}$$

where we have defined $B_{\epsilon,i} := (\epsilon^2 I + S\Sigma_i S^\dagger)$, $i \in \{\star, h\}$. The term (c) was bounded by $Ch^2\|\bar{f}\|_{L^2(D)}$ in the proof of Theorem 3. We now bound terms (d) and (e). For (d) we have:

$$\begin{aligned}\|\Sigma_\star S^\dagger B^{-1}_{\epsilon,\star} - \Sigma_h S^\dagger B^{-1}_{\epsilon,h}\|_{\mathbb{R}^s\to L^2(D)} &\leq \|(\Sigma_\star - \Sigma_h)S^\dagger B^{-1}_{\epsilon,\star}\|_{\mathbb{R}^s\to L^2(D)} \\ &\quad + \|\Sigma_h S^\dagger(B^{-1}_{\epsilon,\star} - B^{-1}_{\epsilon,h})\|_{\mathbb{R}^s\to L^2(D)} \\ &\leq \|\Sigma_\star - \Sigma_h\|_{L^2}\|S\|_{C(D)\to\mathbb{R}^s}\|B^{-1}_{\epsilon,\star}\|_{\mathbb{R}^s\to\mathbb{R}^s} \\ &\quad \underbrace{\|\Sigma_h\|_{L^2}}_{(f)}\|S\|_{C(D)\to\mathbb{R}^s}\underbrace{\|B^{-1}_{\epsilon,\star} - B^{-1}_{\epsilon,h}\|_{\mathbb{R}^s\to\mathbb{R}^s}}_{(g)} \qquad \text{(S31)}\end{aligned}$$

Using Remark 5 we can bound (f) by $\|\Sigma_\star\|_{L^2} + \mathcal{O}(h^2)$. In order to obtain a bound for (g) we first compute:

$$\begin{aligned}\|B_{\epsilon,\star} - B_{\epsilon,h}\|_{\mathbb{R}^s\to\mathbb{R}^s} &= \|S(\Sigma_\star - \Sigma_h)S^\dagger\|_{\mathbb{R}^s\to\mathbb{R}^s} \\ &\leq \|S\|^2_{C(D)\to\mathbb{R}^s}\|\Sigma_\star - \Sigma_h\|_{L^2} \\ &\leq C_1\|S\|^2_{C(D)\to\mathbb{R}^s}h^2 + \mathcal{O}(h^4). \qquad \text{(S32)}\end{aligned}$$

Since $B_{\epsilon,\star}$ and $B_{\epsilon,h}$ are invertible we have for sufficiently small h that $\|B_{\epsilon,\star} - B_{\epsilon,h}\|_{\mathbb{R}^s\to\mathbb{R}^s} < 1/\|B^{-1}_{\epsilon,\star}\|_{\mathbb{R}^s\to\mathbb{R}^s}$ since Eq. (S32) gives us that $\|B_{\epsilon,\star} - B_{\epsilon,h}\|_{\mathbb{R}^s\to\mathbb{R}^s} \leq \mathcal{O}(h^2)$. Thus, we can utilise [S3, Corollary 8.2] to deduce that:

$$\|B^{-1}_{\epsilon,\star} - B^{-1}_{\epsilon,h}\|_{\mathbb{R}^s\to\mathbb{R}^s} \leq \frac{\|B^{-1}_{\epsilon,\star}\|^2_{\mathbb{R}^s\to\mathbb{R}^s}\|B_{\epsilon,\star} - B_{\epsilon,h}\|_{\mathbb{R}^s\to\mathbb{R}^s}}{1 - \|B^{-1}_{\epsilon,\star}\|_{\mathbb{R}^s\to\mathbb{R}^s}\|B_{\epsilon,\star} - B_{\epsilon,h}\|_{\mathbb{R}^s\to\mathbb{R}^s}} \leq C_2h^2 + \mathcal{O}(h^4) \qquad \text{(S33)}$$

where $C_2 := \|B^{-1}_{\epsilon,\star}\|^2_{\mathbb{R}^s\to\mathbb{R}^s}C_1\|S\|^2_{C(D)\to\mathbb{R}^s} > 0$ is a constant independent of h.

Returning to Eq. (S31),

$$\begin{aligned}\|\Sigma_\star S^\dagger B_{\epsilon,\star}^{-1} - \Sigma_h S^\dagger B_{\epsilon,h}^{-1}\|_{\mathbb{R}^s \to L^2(D)} &\leq (C_1 h^2 + \mathcal{O}(h^4))\|S\|_{C(D)\to\mathbb{R}^s}\|B_{\epsilon,\star}^{-1}\|_{\mathbb{R}^s\to\mathbb{R}^s} \\ &\quad + (\|\Sigma_\star\|_{L^2} + \mathcal{O}(h^2))\|S\|_{C(D)\to\mathbb{R}^s}(C_2 h^2 + \mathcal{O}(h^4)) \\ &\leq C_3 h^2 + \mathcal{O}(h^4) \end{aligned} \tag{S34}$$

where $C_3 := C_1\|S\|_{C(D)\to\mathbb{R}^s}\|B_{\epsilon,\star}^{-1}\|_{\mathbb{R}^s\to\mathbb{R}^s} + C_2\|S\|_{C(D)\to\mathbb{R}^s}\|\Sigma_\star\|_{L^2} > 0$ is a constant independent of h. Now returning to Eq. (S30), for (e) we have:

$$\begin{aligned}&\|\Sigma_\star S^\dagger B_{\epsilon,\star}^{-1} S m_\star - \Sigma_h S^\dagger B_{\epsilon,h}^{-1} S m_h\|_{L^2(D)} \\ &\leq \|\Sigma_\star S^\dagger B_{\epsilon,\star}^{-1} S m_\star - \Sigma_\star S^\dagger B_{\epsilon,\star}^{-1} S m_h\|_{L^2(D)} + \|\Sigma_\star S^\dagger B_{\epsilon,\star}^{-1} S m_h - \Sigma_h S^\dagger B_{\epsilon,h}^{-1} S m_h\|_{L^2(D)} \\ &= \|\Sigma_\star S^\dagger B_{\epsilon,\star}^{-1} S(m_\star - m_h)\|_{L^2(D)} + \|(\Sigma_\star S^\dagger B_{\epsilon,\star}^{-1} - \Sigma_h S^\dagger B_{\epsilon,h}^{-1}) S m_h\|_{L^2(D)} \\ &\leq \|\Sigma_\star\|_{L^2}\|S\|_{C(D)\to\mathbb{R}^s}^2\|B_{\epsilon,\star}^{-1}\|_{\mathbb{R}^s\to\mathbb{R}^s}\|m_\star - m_h\|_{L^2(D)} \\ &\quad + \underbrace{\|\Sigma_\star S^\dagger B_{\epsilon,\star}^{-1} - \Sigma_h S^\dagger B_{\epsilon,h}^{-1}\|_{\mathbb{R}^s\to L^2(D)}}_{\text{bound using } Eq.\ (S34)}\|S\|_{C(D)\to\mathbb{R}^s}\underbrace{\|m_h\|_{L^2(D)}}_{Remark\ 5} \\ &\leq \|\Sigma_\star\|_{L^2}\|S\|_{C(D)\to\mathbb{R}^s}^2\|B_{\epsilon,\star}^{-1}\|_{\mathbb{R}^s\to\mathbb{R}^s} C h^2\|\bar{f}\|_{L^2(D)} \\ &\quad + (C_3 h^2 + \mathcal{O}(h^4))\|S\|_{C(D)\to\mathbb{R}^s}(C h^2\|\bar{f}\|_{L^2(D)} + \|m_\star\|_{L^2(D)}) \\ &\leq C_4 h^2 + \mathcal{O}(h^4) \end{aligned} \tag{S35}$$

where $C_4 := C\|\Sigma_\star\|_{L^2}\|S\|_{C(D)\to\mathbb{R}^s}^2\|B_{\epsilon,\star}^{-1}\|_{\mathbb{R}^s\to\mathbb{R}^s}\|\bar{f}\|_{L^2(D)} + C_3\|S\|_{C(D)\to\mathbb{R}^s}\|m_\star\|_{L^2(D)} > 0$ is a constant independent of h. Putting the three bounds together we obtain:

$$\begin{aligned}\|m_{u|\mathbf{v}}^{(\star)} - m_{u|\mathbf{v}}^{(h)}\|_{L^2(D)} &\leq C\|\bar{f}\|_{L^2(D)}h^2 + C_3\|\mathbf{v}\|h^2 + C_4 h^2 + \mathcal{O}(h^4) \\ &= C_5 h^2 + \mathcal{O}(h^4)\end{aligned}$$

where $C_5 := C\|\bar{f}\|_{L^2(D)} + C_3\|\mathbf{v}\| + C_4 > 0$ is a constant independent of h. Thus, the mean term in Eq. (S26) can be bounded, for sufficiently small h, as:

$$\left|\ell m_{u|\mathbf{v}}^{(\star)} - \ell m_{u|\mathbf{v}}^{(h)}\right| \leq C_5\|\ell\|_{L^2(D)\to\mathbb{R}}h^2 + \mathcal{O}(h^4). \tag{S36}$$

For the covariance term in Eq. (S26) it will be useful to make use of the following identity which holds for all $x, y > 0$:

$$|\sqrt{x} - \sqrt{y}| = \frac{|x-y|}{\sqrt{x}+\sqrt{y}}. \tag{S37}$$

This identity follows from writing $x - y = (\sqrt{x} - \sqrt{y})(\sqrt{x} + \sqrt{y})$.

Using identity Eq. (S37) we have:

$$\begin{aligned}\left|\sqrt{\ell\Sigma^{(\star)}_{u|\mathbf{v}}\ell^\dagger}-\sqrt{\ell\Sigma^{(h)}_{u|\mathbf{v}}\ell^\dagger}\right| &= \frac{\left|\ell\Sigma^{(\star)}_{u|\mathbf{v}}\ell^\dagger-\ell\Sigma^{(h)}_{u|\mathbf{v}}\ell^\dagger\right|}{\left|\sqrt{\ell\Sigma^{(\star)}_{u|\mathbf{v}}\ell^\dagger}+\sqrt{\ell\Sigma^{(h)}_{u|\mathbf{v}}\ell^\dagger}\right|}\\ &= \frac{\left|\ell(\Sigma^{(\star)}_{u|\mathbf{v}}-\Sigma^{(h)}_{u|\mathbf{v}})\ell^\dagger\right|}{\left|\sqrt{\ell\Sigma^{(\star)}_{u|\mathbf{v}}\ell^\dagger}+\sqrt{\ell\Sigma^{(h)}_{u|\mathbf{v}}\ell^\dagger}\right|}\\ &\leq \frac{\|\ell\|^2_{L^2(D)\to\mathbb{R}}\|\Sigma^{(\star)}_{u|\mathbf{v}}-\Sigma^{(h)}_{u|\mathbf{v}}\|_{L^2}}{\left|\sqrt{\ell\Sigma^{(\star)}_{u|\mathbf{v}}\ell^\dagger}+\sqrt{\ell\Sigma^{(h)}_{u|\mathbf{v}}\ell^\dagger}\right|}.\end{aligned}$$

In order to proceed with bounding the above we first bound the term involving the difference in posterior covariances as follows:

$$\begin{aligned}\|\Sigma^{(\star)}_{u|\mathbf{v}}-\Sigma^{(h)}_{u|\mathbf{v}}\|_{L^2} &= \|\Sigma_\star-\Sigma_h-\Sigma_\star S^\dagger B^{-1}_{\epsilon,\star}S\Sigma_\star+\Sigma_h S^\dagger B^{-1}_{\epsilon,h}S\Sigma_h\|_{L^2}\\ &\leq \|\Sigma_\star-\Sigma_h\|_{L^2}+\|\Sigma_\star S^\dagger B^{-1}_{\epsilon,\star}S\Sigma_\star-\Sigma_h S^\dagger B^{-1}_{\epsilon,h}S\Sigma_h\|_{L^2}\end{aligned}\tag{S38}$$

The first term above has already been bounded so we focus on the second term and compute:

$$\begin{aligned}&\|\Sigma_\star S^\dagger B^{-1}_{\epsilon,\star}S\Sigma_\star-\Sigma_h S^\dagger B^{-1}_{\epsilon,h}S\Sigma_h\|_{L^2}\\ &\leq \|\Sigma_\star S^\dagger B^{-1}_{\epsilon,\star}S\Sigma_\star-\Sigma_h S^\dagger B^{-1}_{\epsilon,h}S\Sigma_\star\|_{L^2}+\|\Sigma_h S^\dagger B^{-1}_{\epsilon,h}S\Sigma_\star-\Sigma_h S^\dagger B^{-1}_{\epsilon,h}S\Sigma_h\|_{L^2}\\ &\leq \underbrace{\|\Sigma_\star S^\dagger B^{-1}_{\epsilon,\star}-\Sigma_h S^\dagger B^{-1}_{\epsilon,h}\|_{\mathbb{R}^s\to L^2(D)}}_{\text{bound using } Eq.\ (S34)}\|S\|_{C(D)\to\mathbb{R}^s}\|\Sigma_\star\|_{L^2}\\ &\quad+\underbrace{\|\Sigma_h\|_{L^2}}_{Remark\ 5}\|S\|^2_{C(D)\to\mathbb{R}^s}\underbrace{\|B^{-1}_{\epsilon,h}\|_{\mathbb{R}^s\to\mathbb{R}^s}}_{Remark\ 5}\|\Sigma_\star-\Sigma_h\|_{L^2}\\ &\leq C_3\|S\|_{C(D)\to\mathbb{R}^s}\|\Sigma_\star\|_{L^2}h^2\\ &\quad+\|S\|^2_{C(D)\to\mathbb{R}^s}(\|\Sigma_\star\|_{L^2}+\mathcal{O}(h^2))(\|B^{-1}_{\epsilon,\star}\|_{\mathbb{R}^s\to\mathbb{R}^s}+\mathcal{O}(h^2))(C_1h^2+\mathcal{O}(h^2))+\mathcal{O}(h^4)\\ &\leq C_6h^2+\mathcal{O}(h^4)\end{aligned}\tag{S39}$$

where $C_6 := C_3\|S\|_{C(D)\to\mathbb{R}^s}\|\Sigma_\star\|_{L^2}+\|S\|^2_{C(D)\to\mathbb{R}^s}\|\Sigma_\star\|_{L^2}\|B^{-1}_{\epsilon,\star}\|_{\mathbb{R}^s\to\mathbb{R}^s}C_1 > 0$ is a constant independent of h. We can now bound Eq. (S38) as follows:

$$\|\Sigma^{(\star)}_{u|\mathbf{v}}-\Sigma^{(h)}_{u|\mathbf{v}}\|_{L^2}\leq C_7h^2+\mathcal{O}(h^4)\tag{S40}$$

where $C_7 := C_1 + C_6 > 0$ is a constant independent of h. Returning to Eq. (S26):

$$\begin{aligned}
\left|\sqrt{\ell\Sigma^{(\star)}_{u|\mathbf{v}}\ell^\dagger} - \sqrt{\ell\Sigma^{(h)}_{u|\mathbf{v}}\ell^\dagger}\right| &\leq \frac{\|\ell\|^2_{L^2(D)\to\mathbb{R}}\|\Sigma^{(\star)}_{u|\mathbf{v}} - \Sigma^{(h)}_{u|\mathbf{v}}\|_{L^2}}{\left|\sqrt{\ell\Sigma^{(\star)}_{u|\mathbf{v}}\ell^\dagger} + \sqrt{\ell\Sigma^{(h)}_{u|\mathbf{v}}\ell^\dagger}\right|} \\
&\leq \frac{\|\ell\|^2_{L^2(D)\to\mathbb{R}}}{\sqrt{\ell\Sigma^{(\star)}_{u|\mathbf{v}}\ell^\dagger}} \cdot \frac{C_7h^2 + \mathcal{O}(h^4)}{\left|1 + \sqrt{\ell\Sigma^{(h)}_{u|\mathbf{v}}\ell^\dagger}/\sqrt{\ell\Sigma^{(\star)}_{u|\mathbf{v}}\ell^\dagger}\right|} \\
&\leq \frac{C_7\|\ell\|^2_{L^2(D)\to\mathbb{R}}}{\sqrt{\ell\Sigma^{(\star)}_{u|\mathbf{v}}\ell^\dagger}} \cdot h^2 + \mathcal{O}(h^4) \\
&= C_8(\ell)h^2 + \mathcal{O}(h^4) \qquad \text{(S41)}
\end{aligned}$$

where $C_8(\ell) := C_7\|\ell\|^2_{L^2(D)\to\mathbb{R}}/\sqrt{\ell\Sigma^{(\star)}_{u|\mathbf{v}}\ell^\dagger} > 0$ is a constant independent of h (but dependent on ℓ). Note that we have used the fact that both of the posterior variance terms $\ell\Sigma^{(\star)}_{u|\mathbf{v}}\ell^\dagger$ and $\ell\Sigma^{(h)}_{u|\mathbf{v}}\ell^\dagger$ are strictly greater than zero, to arrive at the penultimate line above, since this implies that the denominator is greater than 1. The positivity of the posterior variances follows since both of the posterior covariances are positive definite due to the sensor noise ϵ being strictly positive. Thus, putting the mean and variance bounds together we obtain:

$$\begin{aligned}
W^2(\ell\tilde{\nu}_\star, \ell\tilde{\nu}_\star) &\leq C_5^2\|\ell\|^2_{L^2(D)\to\mathbb{R}}h^4 + C_8(\ell)^2h^4 + \mathcal{O}(h^6) \\
&\leq (C_5^2\|\ell\|^2_{L^2(D)\to\mathbb{R}} + C_8(\ell)^2)h^4 + \mathcal{O}(h^6) \qquad \text{(S42)}
\end{aligned}$$

from which it follows that for sufficiently small h we have:

$$W(\ell\tilde{\nu}_\star, \ell\tilde{\nu}_\star) \leq \gamma'(\ell)h^2 + \mathcal{O}(h^4) \qquad \text{(S43)}$$

where $\gamma'(\ell) := \sqrt{C_5^2\|\ell\|^2_{L^2(D)\to\mathbb{R}} + C_8(\ell)^2} > 0$ is a constant independent of h as claimed. ■

References

[S1] J. Cockayne and A. B. Duncan. Probabilistic gradients for fast calibration of differential equation models. *arXiv preprint arXiv:2009.04239*, 2020.

[S2] M. Girolami, E. Febrianto, G. Yin, and F. Cirak. The statistical finite element method (statFEM) for coherent synthesis of observation data and model predictions. *Computer Methods in Applied Mechanics and Engineering*, 375:113533, Mar. 2021. doi: 10.1016/j.cma.2020.113533. URL https://doi.org/10.1016/j.cma.2020.113533.

[S3] I. Gohberg, S. Goldberg, and M. Kaashoek. *Basic classes of linear operators*. Birkhäuser, 2012.

[S4] A. M. Stuart. Inverse problems: a bayesian perspective. *Acta numerica*, 19:451–559, 2010.